AD-A154 899 A SIMULATION OF THE NAVIGATION AND ORIENTATION POTENTIAL OF THE GEOSTAR RECEIVER(U) NAVAL SURFACE WEAPONS CENTER DAHLGREN VA B R HERMANN OCT 83 1/1

UNCLASSIFIED NSWC/TR-83-377 F/G 17/7 NL

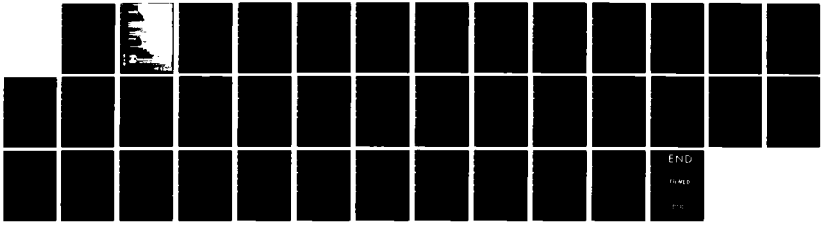

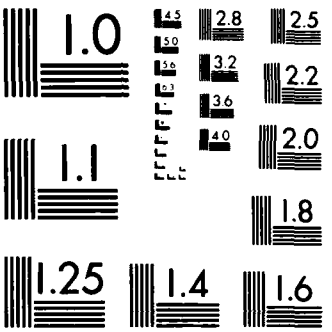

UNCLASSIFIED

SECURITY CLASSIFICATION OF THIS PAGE *(When Data Entered)*

REPORT DOCUMENTATION PAGE

READ INSTRUCTIONS BEFORE COMPLETING FORM

1. REPORT NUMBER: NSWC TR 83-377	2. GOVT ACCESSION NO. A154899
3. RECIPIENT'S CATALOG NUMBER	
4. TITLE *(and Subtitle)*: A SIMULATION OF THE NAVIGATION AND ORIENTATION POTENTIAL OF THE GEOSTAR RECEIVER	5. TYPE OF REPORT & PERIOD COVERED: Final
	6. PERFORMING ORG. REPORT NUMBER
7. AUTHOR(s): Bruce R. Hermann	8. CONTRACT OR GRANT NUMBER(s)
9. PERFORMING ORGANIZATION NAME AND ADDRESS: Naval Surface Weapons Center (K13), Dahlgren, VA 22448	10. PROGRAM ELEMENT, PROJECT, TASK AREA & WORK UNIT NUMBERS: 63701B
11. CONTROLLING OFFICE NAME AND ADDRESS: Defense Mapping Agency Headquarters, 6500 Brookes Lane, Washington, DC 20315	12. REPORT DATE: October 1983
	13. NUMBER OF PAGES: 39
14. MONITORING AGENCY NAME & ADDRESS *(if different from Controlling Office)*	15. SECURITY CLASS. *(of this report)*: UNCLASSIFIED
	15a. DECLASSIFICATION/DOWNGRADING SCHEDULE

16. DISTRIBUTION STATEMENT *(of this Report)*

Approved for public release; distribution unlimited.

17. DISTRIBUTION STATEMENT *(of the abstract entered in Block 20, if different from Report)*

18. SUPPLEMENTARY NOTES

19. KEY WORDS *(Continue on reverse side if necessary and identify by block number)*

Global Positioning System (GPS)
Three-Dimensional Navigation Fixes
GEOSTAR Navigation Processor
Bias Residual
Navigation Residual
Orientation Residual
Offset Residual

20. ABSTRACT *(Continue on reverse side if necessary and identify by block number)*

A computer simulation was performed to demonstrate that the signals from the Global Positioning System (GPS) satellites are able to provide a user with sufficient information to navigate and orient a moving vehicle. A particular application of interest is the orientation of a slowly moving survey ship. Orientation accuracies on the order of 0.1 mrad and positions within 20 m RSS are desired.

DD FORM 1 JAN 73 1473 EDITION OF 1 NOV 65 IS OBSOLETE
S/N 0102-LF-014-6601

UNCLASSIFIED

SECURITY CLASSIFICATION OF THIS PAGE *(When Data Entered)*

FOREWORD

The Global Positioning System (GPS) is being developed primarily for the purpose of providing a user with accurate three-dimensional navigation fixes anywhere near the surface of the earth. This system has many unique characteristics that make it useful for other applications as well. One of these is the capability of providing the user with orientation information if he is able to receive signals from several antennas simultaneously.

This report describes a preliminary investigation of the potential for simultaneous, real time, navigation and orientation solutions using time-multiplexed GPS receiver technology such as the Texas Instruments (TI) GEOSTAR. Computer-generated data was used to simulate the gross characteristics of the GEOSTAR. This data was then processed with a least-squares algorithm to provide the desired solutions.

Support for this simulation was provided by the Eastern Space and Missile Center, Patrick Air Force Base, Cocoa Beach, Florida.

This report was reviewed and approved by R. W. Hill, Head, Space Flight Sciences Branch; and Carlton W. Duke, Jr., Head, Space and Surface Systems Division.

Released by:

T. A. CLARE, HEAD
Strategic Systems Department

CONTENTS

FIGURES

TABLES

PLOTS

IMPLEMENTATION

Three-dimensional orientation requires at least three independent antennas to define a plane. Four non-coplanar antennas could be used to define two planes and provide redundancy. Orientation solutions of the planes containing the antennas are related to the vehicle and, therefore, allow the orientation of the vehicle to be determined. The vehicle position can be obtained from pseudoranges in a manner similar to the conventional navigation solution if four GPS satellites are in view[1]. Four satellites will also add strength to the orientation solution. For these reasons, and algorithm simplicity, this simulation requires that four satellites always be in view. Operational versions of this software will need to be able to handle cases where fewer than four satellites are available, but this complication will be deferred pending the results of the current simulation.

The TI GEOSTAR[2] receiver has eight software trackers available. These are intended to be used to track four satellites on both L band frequencies simultaneously. The two frequency measurements provide the means to correct for the propagation effects due to ionospheric refraction. If the receiver were operated on a single frequency, there would, in principle, be enough trackers available to allow four satellites to be tracked by two antennas. Assuming that the antennas are not separated by more than a few tens of meters, the loss of L2 would not affect the orientation solution appreciably. However, the position solution would be adversely affected; for this reason alone, two-frequency operations will probably be required.

The desirability of two-frequency observations from four satellites implies that a complete GEOSTAR receiver needs to be dedicated to each antenna. Since at least three antennas are required, three GEOSTARs feeding a single processing computer will be necessary. This is probably an extravagant use of hardware, but it may be necessary to realize the precision desired.

An alternative might take advantage of the similarity of the signal dynamics received from each antenna. The GEOSTAR has a fundamental clocking interval (T) of 20 ms duration. All receiver operations are some integer fraction or multiple of T. Typically, the GEOSTAR dwells for T/2 ms on each satellite and T/4 on each frequency of a particular satellite. Thus, it has completed an observation cycle (two frequencies and four satellites) after 2T ms[1]. If the antennas were connected to a single GEOSTAR via an RF switch that operated in synchronism with the GEOSTAR cycle, then a new antenna could be switched on line every 2T ms. Since the signal dynamics will be similar from each antenna, reacquisition of the same four satellites via the new antenna using the GEOSTAR receiver software should not be difficult. Thus, it might be possible to keep three or four auxiliary sets of tracking loops (one per antenna) running in the navigation processor, each set being updated by the receiver processor or software. Update intervals of the trackers in the GEOSTAR navigation processor would then be 2NT ms, where N is the number of antennas being utilized.

Several variations of this scheme may be possible. The trackers in the navigation processor might be duplicates of the receiver processor trackers, except that they would be updated less frequently. They could also be difference trackers; again taking advantage of the similarity of signal dynamics. In this case, one antenna

would be the reference and its tracker would follow the full-signal dynamics. The other trackers would just track the difference between the dynamics received by its antenna and the reference. These difference trackers would not need frequent updates and so the more critical reference trackers could be updated in alternate 2T-ms intervals. The antenna switching sequence might be ABACADAB . . . where antenna A is the designated reference. In this operating mode, the GEOSTAR navigation processor would be busy tracking signals and, consequently, an outboard computer would be required to perform the real-time position and orientation solutions.

In either mode of operation, each tracker will be updated at a regular but different interval. Consequently, it will be necessary to propagate the current state of each tracker to a common future time. The error involved in this operation is small in low-dynamic applications, and it has the important benefit of providing simultaneous observations from all trackers at each requested observation time. The simulation uses this property and, therefore, requires that all observations occur simultaneously at a time tag obtained from the local clock.

The broadcast ephemeris and satellite clock correction from each satellite are used to compute the earth-fixed coordinates. These ephemeris parameters are assumed by the simulation to be correct. There are no compensating parameters in the state vector. However, the local clock offset is unknown and is a parameter in the state vector. Also unknown are antenna biases. These states model the differences in cable length between the various antennas and the receiver. These differential cable delays need not be calibrated as long as they can be modeled by a linear polynomial of the form

$$p(t) = a_0 + a_1(t - t_0)$$

However, it is assumed that there are no unexpected discontinuities that might influence the coefficients a_0 and a_1 during the period of observation. There is the possibility that certain other effects (e.g., interchannel biases in multihardware-channel receivers) may behave like antenna biases over the short term, but may not be properly modeled by p(t) over the long term. In the GEOSTAR, there is only one hardware channel and whenever a new satellite is acquired, it is presumed that the phase observations from the new satellite are consistent with the old and not randomized by an arbitrary phase offset. If experience demonstrates that this condition cannot be met, then a new antenna bias will have to be defined whenever a different satellite is selected.

CONDITIONS OF THE SIMULATION

The observation error has been selected on the basis of the information in the TI Design Analysis Report III[4] and two-frequency operation. The GEOSTAR observation errors follow:

Pseudorange: L_1 = 0.687 m RSS
L_2 = 0.768 m RSS
Ionospherically Corrected Pseudorange = 2.11 m

Phase: (P Code Tracking): L_1 = 0.147 cm RSS
L_2 = 0.199 cm RSS
Ionospherically Corrected Phase = 0.48 cm

$$\sigma_\rho^2 = 6.48\,\sigma_{L_1}^2 + 2.39\,\sigma_{L_2}^2$$

All simulated observations are free from tropospheric refraction and relativity effects; however, flicker noise has been added to model the expected random variations due to the local frequency standard. The simulation assumptions follow:

1. Four satellites always available
2. Observation errors: Pseudorange $\sigma = 2$ m
   Phase $\sigma = 0.005$ m
3. All observations simultaneous
4. Satellite ephemeris and time corrections contain no error
5. Antenna baseline length and orientation with respect to vehicle unknown
6. Antenna biases modeled by bias and drift
7. Tropospheric refraction and relativity neglected
8. Receiver tracker phase does not randomize when switching satellites

The GPS satellite constellation used in the simulation was the 18-satellite, 6-plane system. The right ascension of the ascending nodes of the constellation are separated by 60 deg, with the satellites within a plane separated by 120 deg. The phasing of satellites in adjacent planes is offset by 40 deg.[5] The orbital period is the standard 11.966 hr, eccentricity was selected as 0.001, and the inclination of each plane was 55 deg. Figure 1 shows the look angles from the receiver to the five satellites in view during the simulation. Of these five satellites, 7, 10, 15, and 17 produced the best Geometric Dilution of Precision (GDOP) and were the four for which synthetic data was generated.

ESTIMATOR

The data processing was performed by a least-squares batch estimator using both the pseudorange and phase data from all antennas at each observation time. Two classes of states are employed in the solution. The first class includes all time-dependent states: the vehicle earth-fixed coordinates (x, y, and z), the vehicle orientation with respect to the local vertical (roll, pitch, and yaw), and the local clock offset. These states are estimated solely from the data obtained at a single observation time and are independent of previous results in all respects with the exception of the correlations that exist between the first and second class of states.

The second class of states include the antenna biases that are assumed to be independent of time. This assumption allows all previous data to be employed at each observation time of these states. The accumulation of data is accomplished by eliminating, in a formal elimination procedure at each observation time, the first class of states. The results of the elimination are then saved and accumulated through the entire simulation. The matrix manipulations leading to the solution are described in Appendix A.

Since the vehicle position and orientation are members of the state vector and the data is collected by several antennas with positions that are not states, it is required that the location of the antennas in the vehicle coordinate system be accurately known beforehand. The assumption requires that these locations can be surveyed with a precision better than the phase measurement accuracy so that they do not contribute to the orientation errors. A description of the various coordinate transformations that are required is presented in Appendix B.

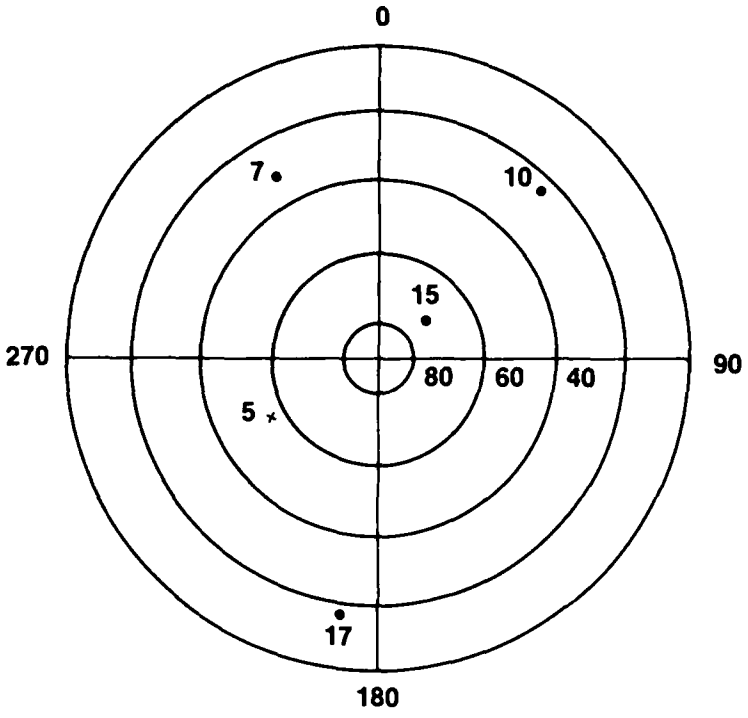

GDOP = 2.8

SAT	NODE	m + ω	AZIMUTH	ELEVATION
5	90	160	241.9	56.4
7	150	80	319.6	30.4
10	210	120	55.0	23.6
15	270	40	60.6	71.7
17	330	320	187.1	18.9

FIGURE 1. SATELLITE SELECTION FOR SIMULATION

SIMULATION

Simulated pseudorange and phase data were generated for these antennas at 6-s intervals for a span of 720 s. Vehicle motion was at a constant velocity of 2.54 m/s and a constant heading of 127.8 deg. Sinusoidal roll, pitch, and yaw signals of different periods and amplitudes were introduced as perturbations. The heading was added directly to the yaw signal. The local clock was offset from GPS time by 50 μs with a drift of 1 ns/s. Added to this offset was the flicker noise process that models the random variations of the local crystal frequency standard[6]. Antenna biases were also introduced on all antennas except the reference. The biases for the reference are assumed to be included in the local clock offsets. All the conditions of the simulation are summarized below:

Dynamic Cases: Time Step = 6 s; Time Span = 720 s

Baseline System Translation and Rotation: $V_{b_x} = -0.61$; $\theta_1 = -45°$
$V_{b_y} = +10.36$ $\theta_2 = -5°$
$V_{b_z} = +20.73$

True States: Longitude = 282° + 0.000018° t
Latitude = 28° − 0.000014° t
Height = 0 m
Roll = 5° * sin (2π * 0.01) t
Pitch = 10° * sin (2π * 0.03) t
Yaw = 8° * sin (2π * 0.02) t
Clock Bias = 50 μs + 1 ns s + flicker
Antenna 2 = 2.9979 m
Antenna 3 = 5.9957 m
Antenna 4 = −2.9979 m
Flicker: τ_1 = 1; τ_2 = 100; $\tau_3 = 10^6$; $\tau_4 = 10^{11}$

The results from two cases will be presented. Both use all the same conditions, except that the antenna baseline lengths are different by a factor of 10. In both cases, the antennas are located in a coordinate system offset from the vehicle by the vector V_b and rotated in azimuth by θ_1 and in elevation by θ_2. The antenna locations (meters) in this rotated system are as follows:

Case 1:	0, 0, 0	*Case 2:* 0, 0, 0
	2, 0, 2	20, 0, 20
	0, 2, 2	0, 20, 20

RESULTS

The initial conditions given the estimator, vs the true conditions, are tabulated in Table 1. The given conditions were offset from the truth by 2 deg in longitude and 2 deg in latitude. The heading or yaw angle was in error by 37.8 deg. These offsets were included to demonstrate the rapid convergence to the true solution as is illustrated in the residual plots. Both the navigation solution and the orientation solution converge within the first few observation intervals.

TABLE 1. INITIAL CONDITIONS OF THE SIMULATION

	True Initial Conditions	Given Initial Conditions
Longitude (deg)	282	280
Latitude (deg)	28	26
Height (m)	0	0
Roll (deg)	0	0
Pitch (deg)	0	0
Yaw (deg)	127.8	90
Biases		
Local Clock (μs)	50	0
Antenna 2 (ns)	10	0
Antenna 3 (ns)	20	0
Antenna 4 (ns)	−10	0

The performance of the estimator is evaluated by comparing the estimated solution for each state with the true value at each observation time. The difference (estimate-truth) and the standard deviations of various states are plotted. The average values of the residuals, the RMS of the residuals over the entire 720-s span, and the standard deviation at the end of the simulation are given in Table 2. Plots 1-9 illustrate the residuals from Case 1 and Plots 11-19 are residuals from Case 2. The plots are semilog with GPS time the linear horizontal axis and the residuals plotted on the vertical log axis. The standard deviations at each time are plotted as heavy solid lines and, in most cases, bracket the residual values that are plotted as "o" symbols.

TABLE 2. AVERAGE, RMS, AND STANDARD DEVIATION OF THE RESIDUALS OVER THE ENTIRE 720-S OBSERVATION SPAN

CASE 1: 3 ANTENNAS, 2-M BASELINES

State	Average	RMS	S.D.
x (m)	0.096	1.345	1.315
y (m)	- 0.181	2.052	2.392
z (m)	0.029	1.324	1.289
roll (rad)	- 0.000262	0.002004	0.002063
pitch (rad)	0.000336	0.002474	0.001934
yaw (rad)	- 0.000114	0.002374	0.002671
clock (m)	- 0.040	1.354	1.533

CASE 2: 3 ANTENNAS, 20-M BASELINES

x (m)	0.090	1.340	1.314
y (m)	- 0.185	2.052	2.392
z (m)	0.026	1.321	1.289
roll (rad)	+0.000035	0.000386	0.000206
pitch (rad)	0.000245	0.000739	0.000193
yaw (rad)	+0.000076	0.000610	0.000267
clock (m)	- 0.044	1.354	1.533

If the estimator has done its job properly, the residual plots of all Class 1 states should contain no systematic signals or trends. If the estimator has modeled the physical system correctly, the residuals should be representative of the noise processes that are inherent in the measurement and reflected in the states. Class 2 states, the antenna biases, are correlated from observation to observation due to the accumulation process. Consequently, the Class 2 residuals show considerable correlation as they hunt for the zero residual level.

Plots 1-3 and 11-13 show the navigation residuals in the two cases. The change in baseline length has little effect upon the navigation solution or upon the local clock offset (Plots 7 and 17). This result is expected, since navigation can be performed with a single antenna. The orientation residuals are shown in Plots 4-6 and 14-16. The improvement with the longer baseline (Case 2) is readily apparent. The standard deviations of the three orientations approach 0.002 rad in Case 1 and 0.0002 rad in Case 2. By employing the assumptions of this

The construction of this A matrix is pursued in the next section of this appendix.

Batch least squares proceeds by rewriting equation (A-1) and then premultiplying by $A^T W$

$$A\Delta\bar{x}_k = (\square - C)_k$$

$$A^T W A \Delta\bar{x}_k = A^T W (\square - C)_k \tag{A-2}$$

The matrix W is a weight matrix that weighs the two data classes appropriately. This expression can be simplified by letting

$$B = A^T W A$$

and

$$E = \square - C$$

Next, the B matrix is partitioned to allow for two classes of states: Class 1 is represented by the states $\Delta\bar{x}_p$ and Class 2 by the states $\Delta\bar{x}_b$. The partitioning is as follows:

$$B = \begin{vmatrix} B_{pp} & B_{pb} \\ B_{pb}^T & B_{bb} \end{vmatrix}, \Delta\bar{x} = \begin{vmatrix} \Delta\bar{x}_p \\ \Delta\bar{x}_b \end{vmatrix}, E = \begin{vmatrix} E_p \\ E_b \end{vmatrix} \tag{A-3}$$

Substitution of equation (A-3) into equation (A-2) produces the following two simultaneous matrix equations:

$$B_{pp}\Delta\bar{x}_p + B_{pb}\Delta\bar{x}_b = E_p \tag{A-4}$$

$$B_{pb}^T \Delta\bar{x}_p + B_{bb}\Delta\bar{x}_b = E_b \tag{A-5}$$

Class 1 states are eliminated by solving equation (A-4) for $\Delta\bar{x}_p$:

$$\Delta\bar{x}_p = B_{pp}^{-1}(E_p - B_{pb}\Delta\bar{x}_b)$$

Substitution of this result into equation (A-5) produces the matrix equation

$$(B_{bb} - B_{pb}^T B_{pp}^{-1} B_{pb})\Delta\bar{x}_b = E_b - B_{pb}^T B_{pp}^{-1} E_p \tag{A-6}$$

This equation is independent of the Class 1 states $\Delta\bar{x}_p$. If equation (A-6) is summed over all observations up to the present, it carries all the information acquired about the Class 2 states.

$$D_{k-1} = \sum_{i=1}^{k-1} [B_{bb} - B_{pb}^T B_{pp}^{-1} B_{pb}]$$

$$F_{k-1} = \sum_{i=1}^{k-1} [E_b - B_{pb}^T B_{pp}^{-1} E_p]$$

These accumulated matrices can then be used along with the data from the most recent observation at t_k to estimate the current state. This final form is as follows:

APPENDIX A

BATCH LEAST SQUARES FORMULATION

MATRIX MANIPULATIONS

The observations used in this simulation consist of (1) pseudoranges from each GPS satellite to each antenna and (2) phase differences between each antenna and the reference antenna from each of the satellites. If there are n_s satellites and n_a antennas, the number of observations at each time step t_k is

$$n_s (2n_a - 1)$$

At each time step, there will exist an estimate of each observatio. based upon previous information. If the actual observations are represented by the column vector $\square_k$ and tne estimate of the observations by C_k, then the difference provides information about the error in the estimate. The parameters of interest are the states $\bar{X}_k$, and since C_k is computed from estimates of these states at each time step, the error in the estimate provides information to correct the states. The formulation that adjusts the states to match the observations begins by expanding C_k by use of Taylor's Series around the current state estimate $\hat{X}_k$. The general expression for the expansion follows:

$$\square_k = C_k + \frac{\partial C_k}{\partial \hat{x}_k} (x_k - \hat{x}_k) + \frac{1}{2!} \frac{\partial^2 C_k}{\partial \hat{x}_k^2} (\bar{x}_k - \hat{x}_k)^2 + \ldots + \frac{1}{n!} \frac{\partial^n C_k}{\partial \hat{x}_k^n} (\bar{x}_k - \hat{x}_k)^n$$

In order to employ linear estimation theory, this expression must be approximated by truncating the series after the term involving the first partial derivative. Then, C_k is moved to the left hand side of the equality and what remains is the linear approximation.

$$\square_k - C_k = \frac{\partial C_k}{\partial \hat{x}_k} (x_k - \hat{x}_k) \qquad \text{(A-1)}$$

The matrix of partial derivatives $\partial C_k / \partial X_k$ is generally known as the "A" matrix:

$$A_k = \left| \frac{\partial C}{\partial \hat{x}_1} \quad \frac{\partial C}{\partial \hat{x}_2} \quad \frac{\partial C}{\partial \hat{x}_3} \quad \ldots \quad \frac{\partial C}{\partial \hat{x}_j} \right|_k$$

The subscript j represents the number of states in the solution and k is the time step. The difference between the true and estimated state will be designated by the vector $\Delta \bar{x}_k$, where

$$\Delta \bar{x}_k = \bar{x}_k - \hat{x}_k$$

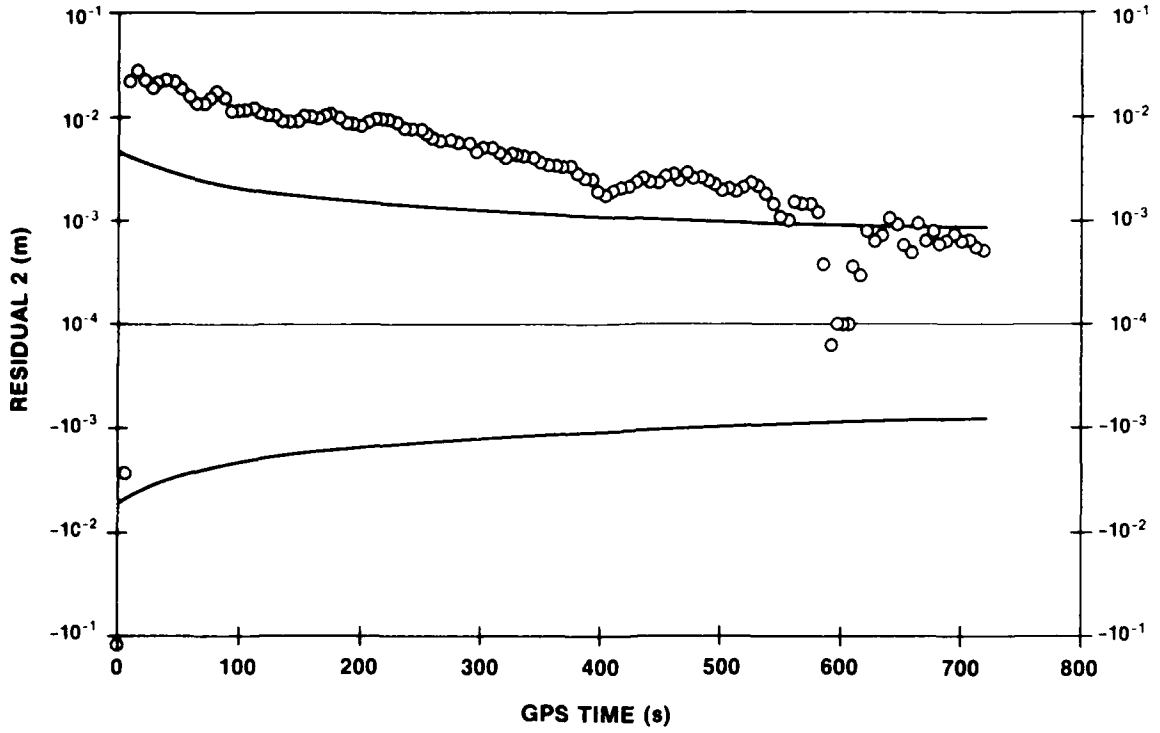

PLOT 18. ANTENNA 2 BIAS RESIDUALS (ESTIMATE-TRUTH); 20-m ANTENNA BASELINES

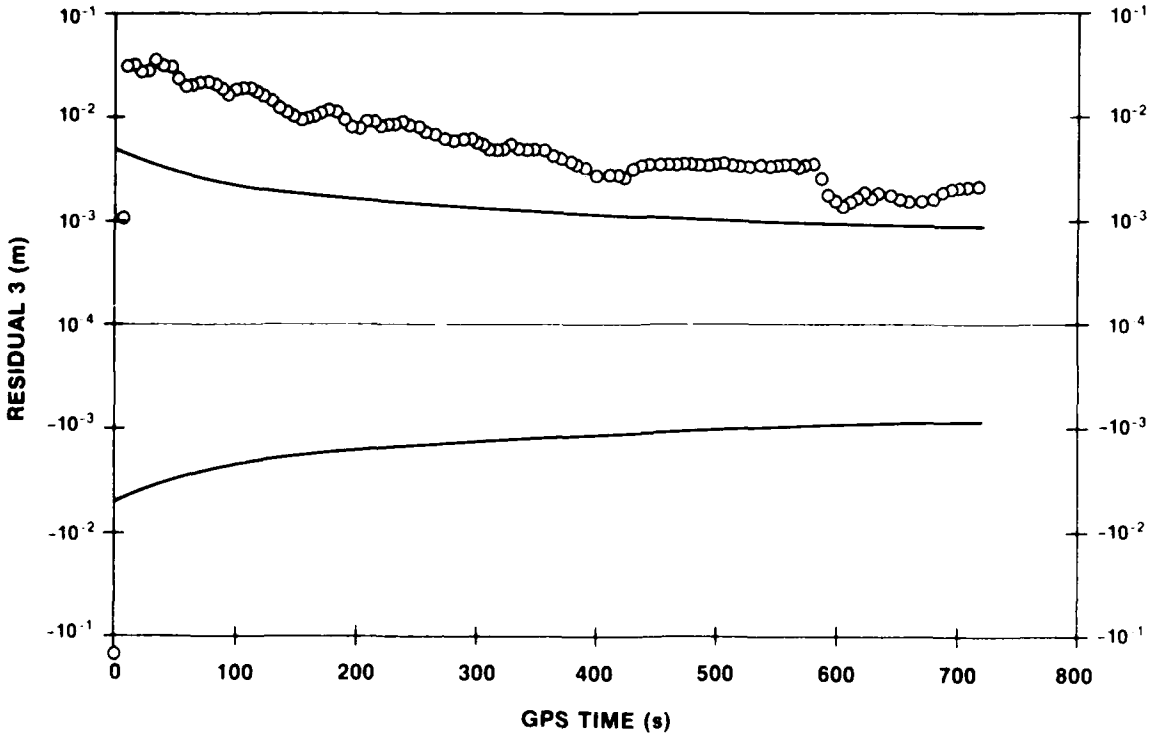

PLOT 19. ANTENNA 3 BIAS RESIDUALS (ESTIMATE-TRUTH); 20-m ANTENNA BASELINES

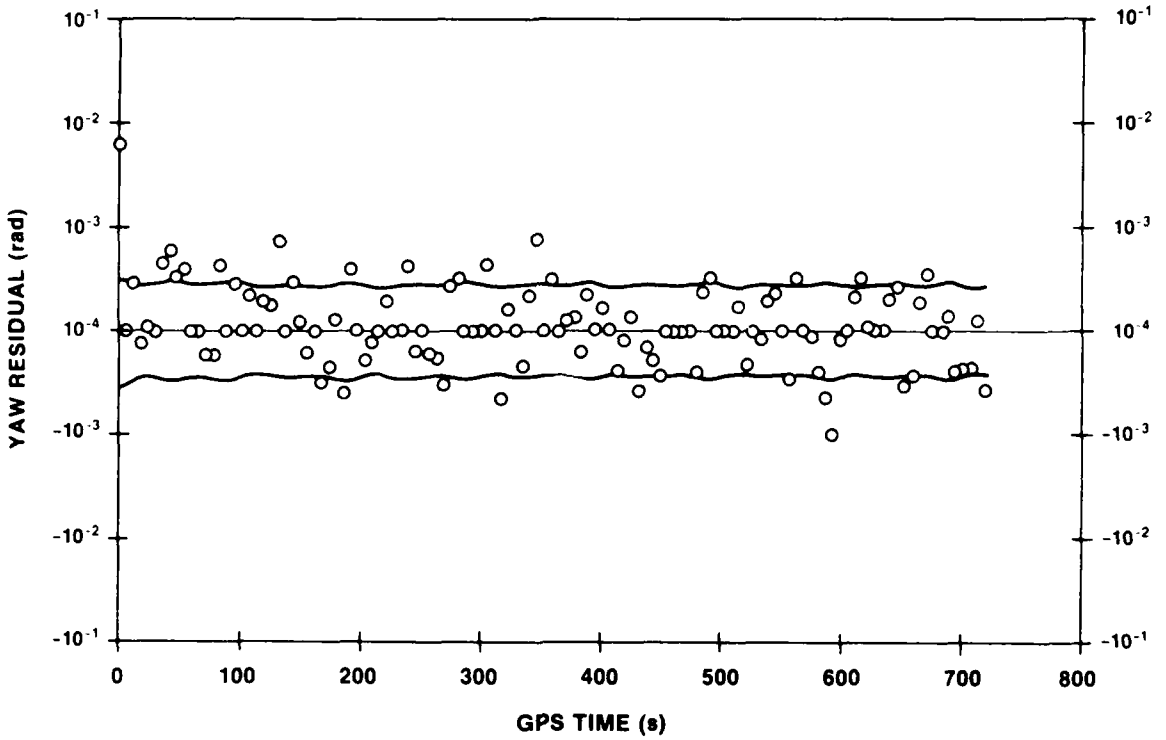

PLOT 16. ORIENTATION RESIDUALS, LOCAL VERTICAL YAW (ESTIMATE-TRUTH); 20-m ANTENNA BASELINES

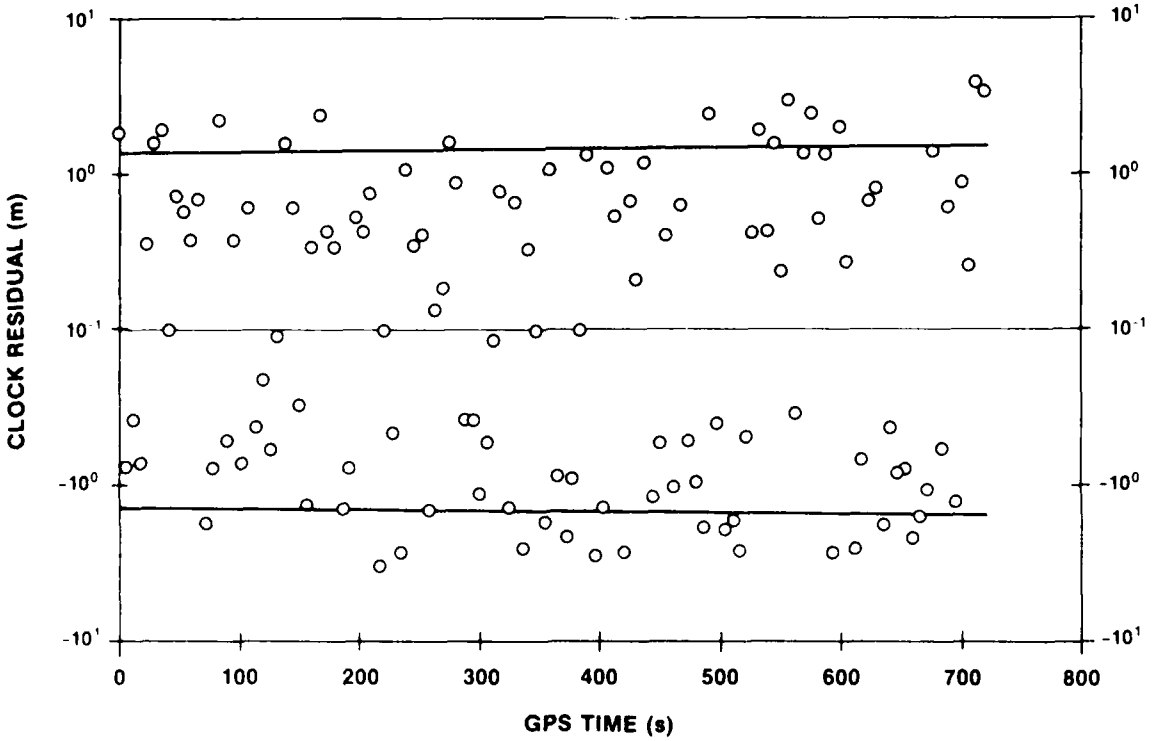

PLOT 17. LOCAL CLOCK OFFSET RESIDUALS (ESTIMATE-TRUTH); 20-m ANTENNA BASELINES

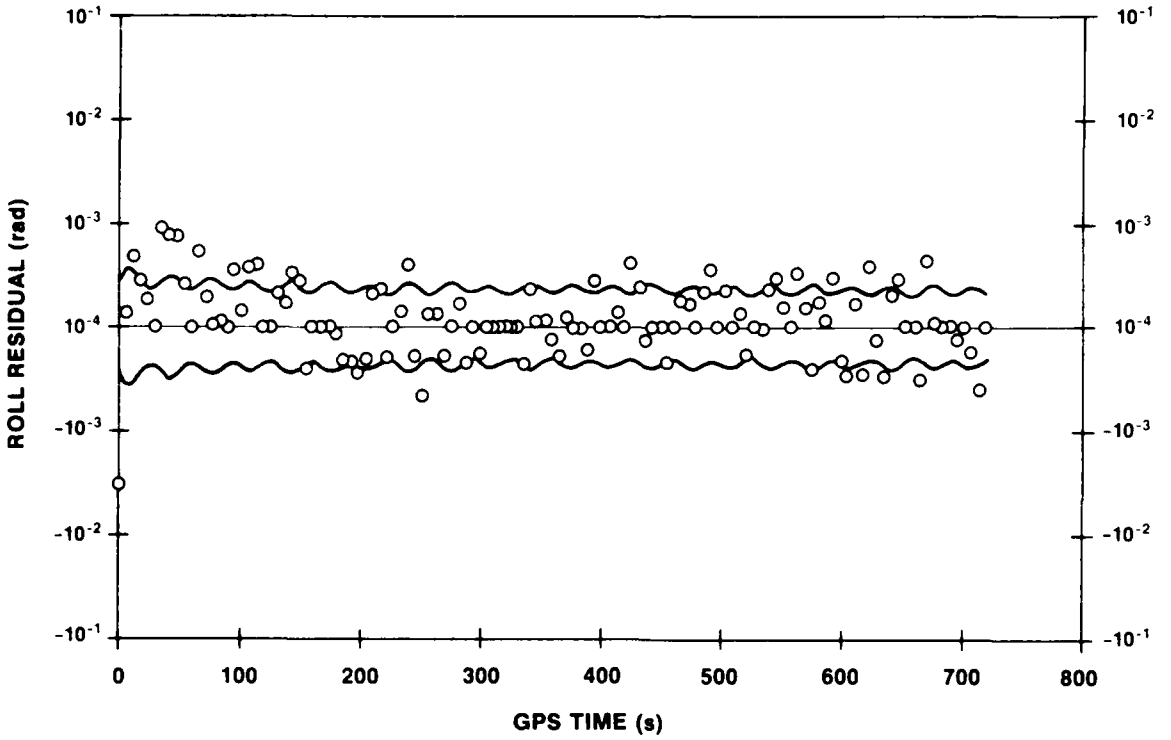

PLOT 14. ORIENTATION RESIDUALS, LOCAL VERTICAL ROLL (ESTIMATE-TRUTH); 20-m ANTENNA BASELINES

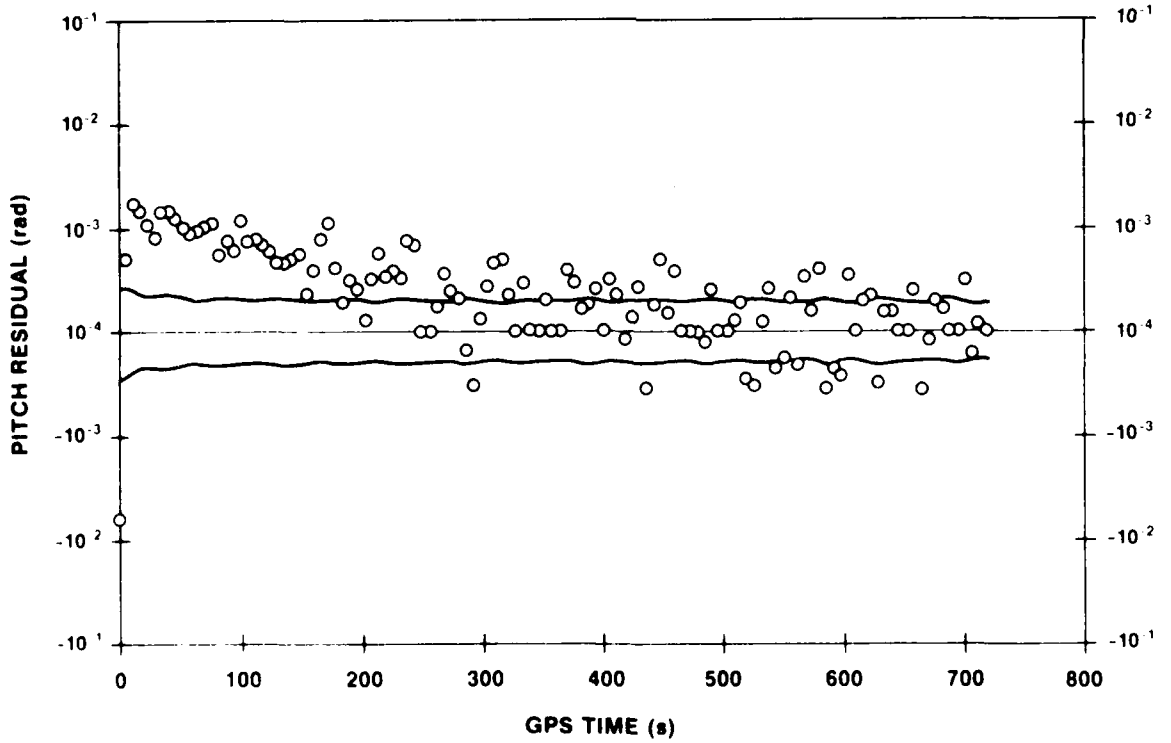

PLOT 15. ORIENTATION RESIDUALS, LOCAL VERTICAL PITCH (ESTIMATE-TRUTH); 20-m ANTENNA BASELINES

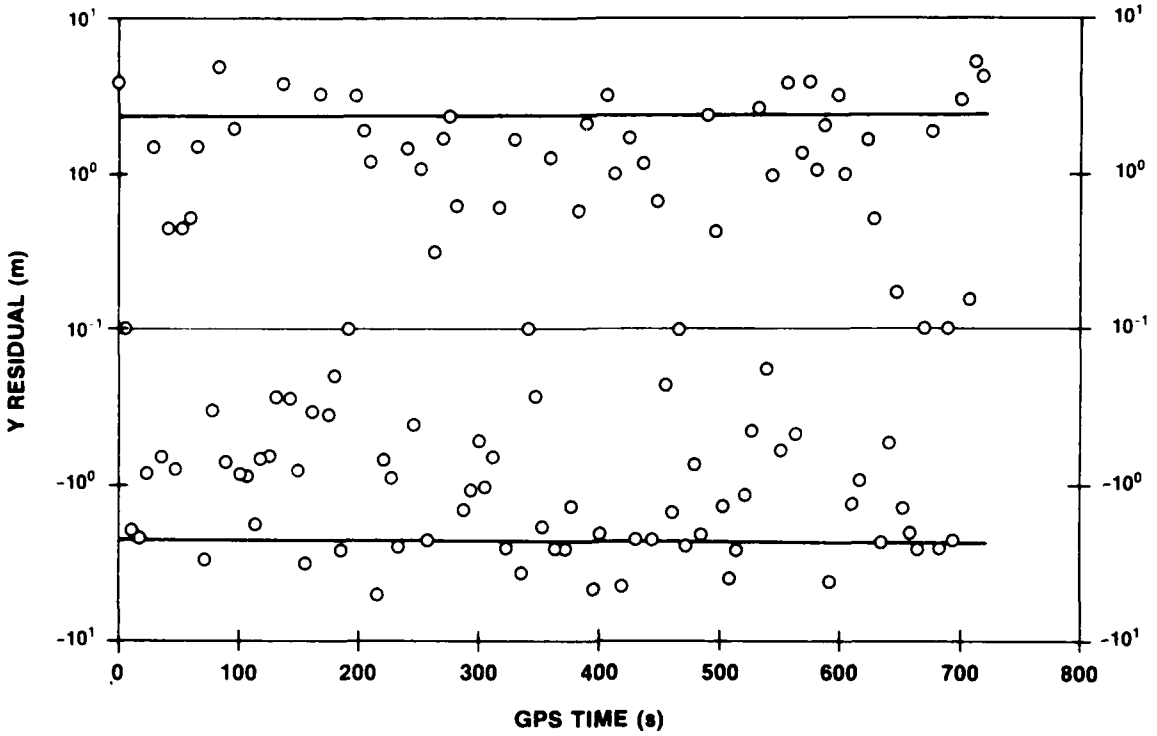

PLOT 12. NAVIGATION RESIDUALS, EARTH-FIXED Y (ESTIMATE-TRUTH); 20-m ANTENNA BASELINES

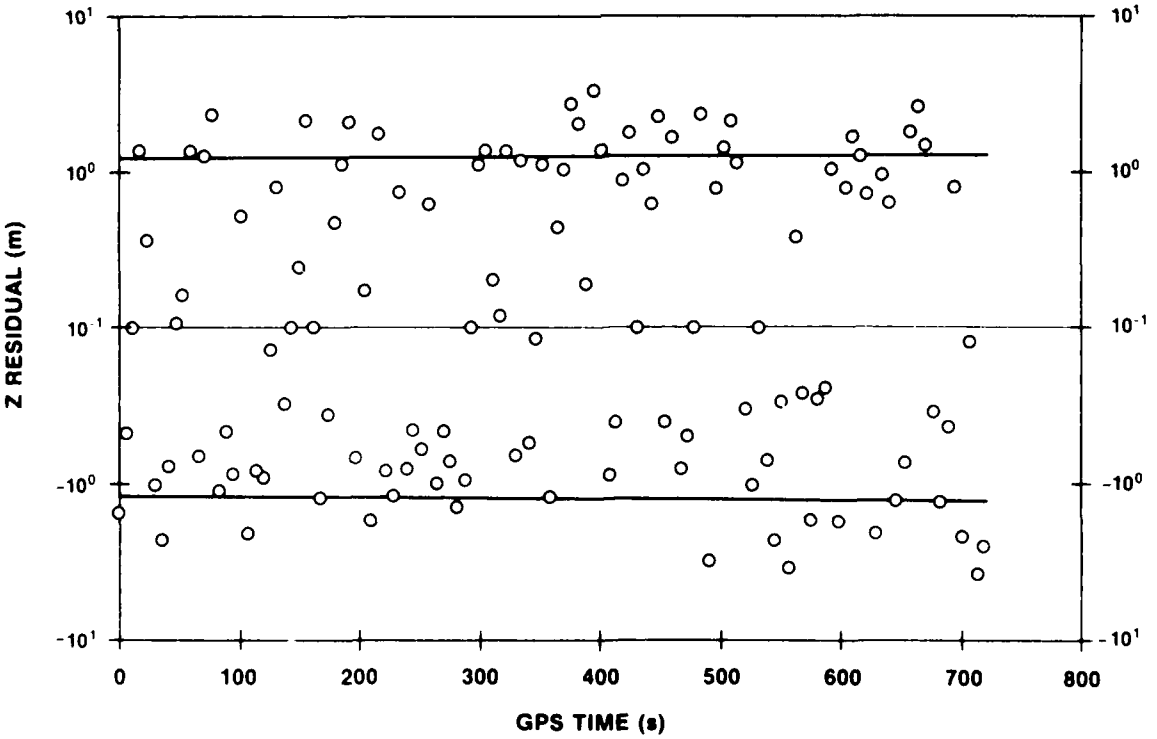

PLOT 13. NAVIGATION RESIDUALS, EARTH-FIXED Z (ESTIMATE-TRUTH); 20-m ANTENNA BASELINES

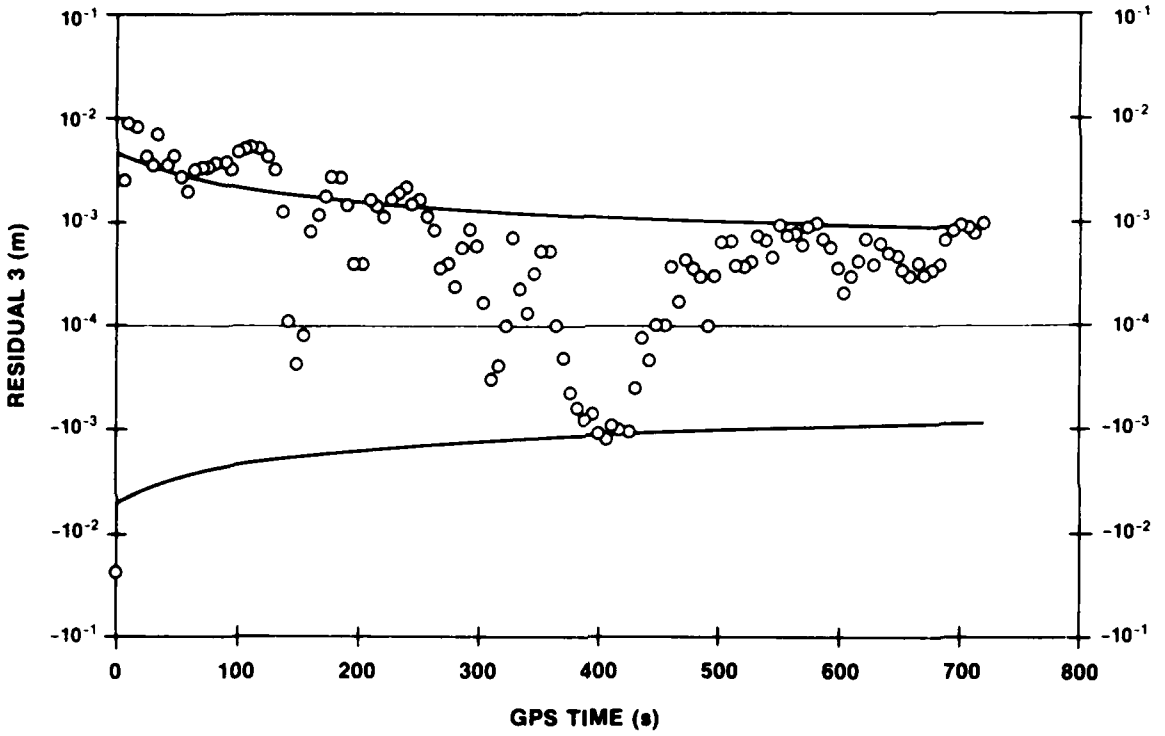

PLOT 9. ANTENNA 3 BIAS RESIDUAL (ESTIMATE-TRUTH); 2-m ANTENNA BASELINES

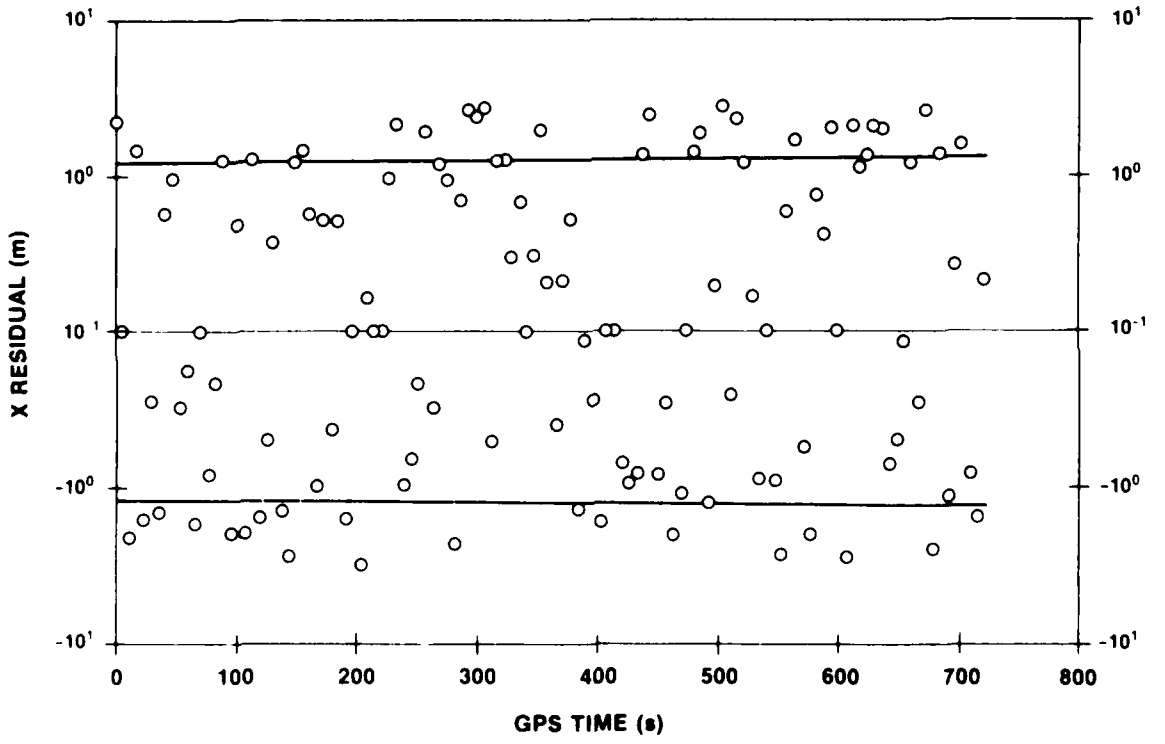

PLOT 11. NAVIGATION RESIDUALS, EARTH-FIXED X (ESTIMATE-TRUTH); 20-m ANTENNA BASELINES

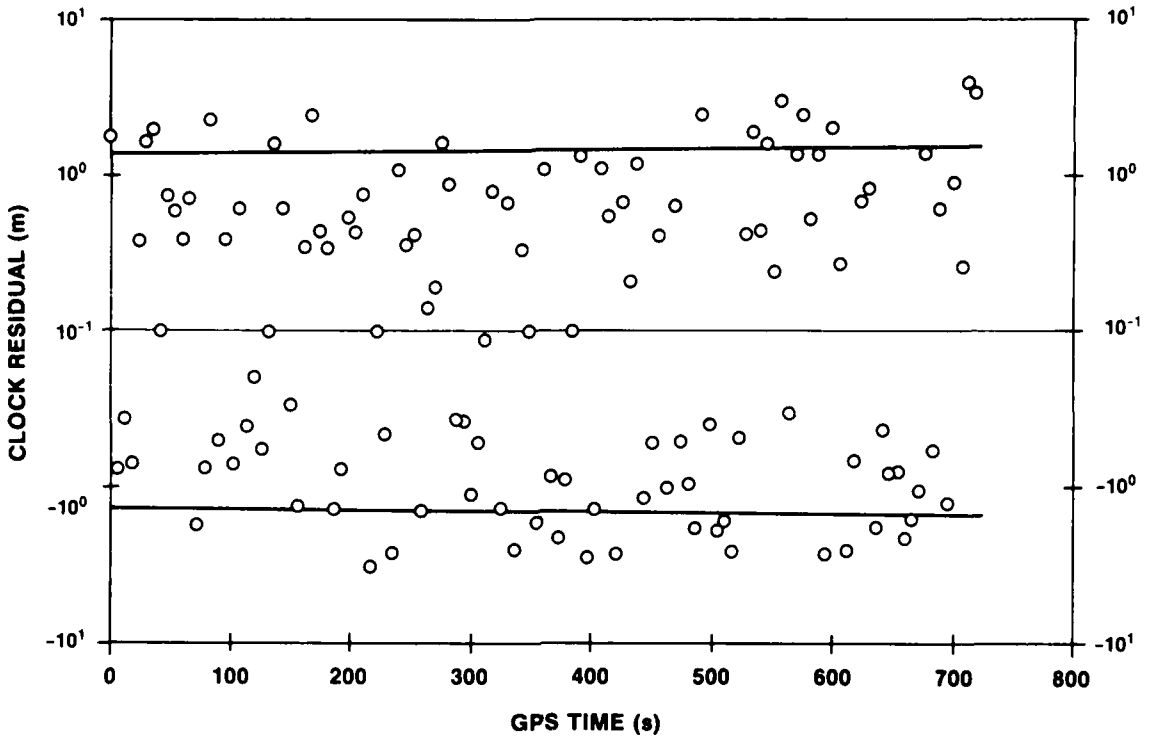

PLOT 7. LOCAL CLOCK OFFSET RESIDUALS, (ESTIMATE-TRUTH); 2-m ANTENNA BASELINES

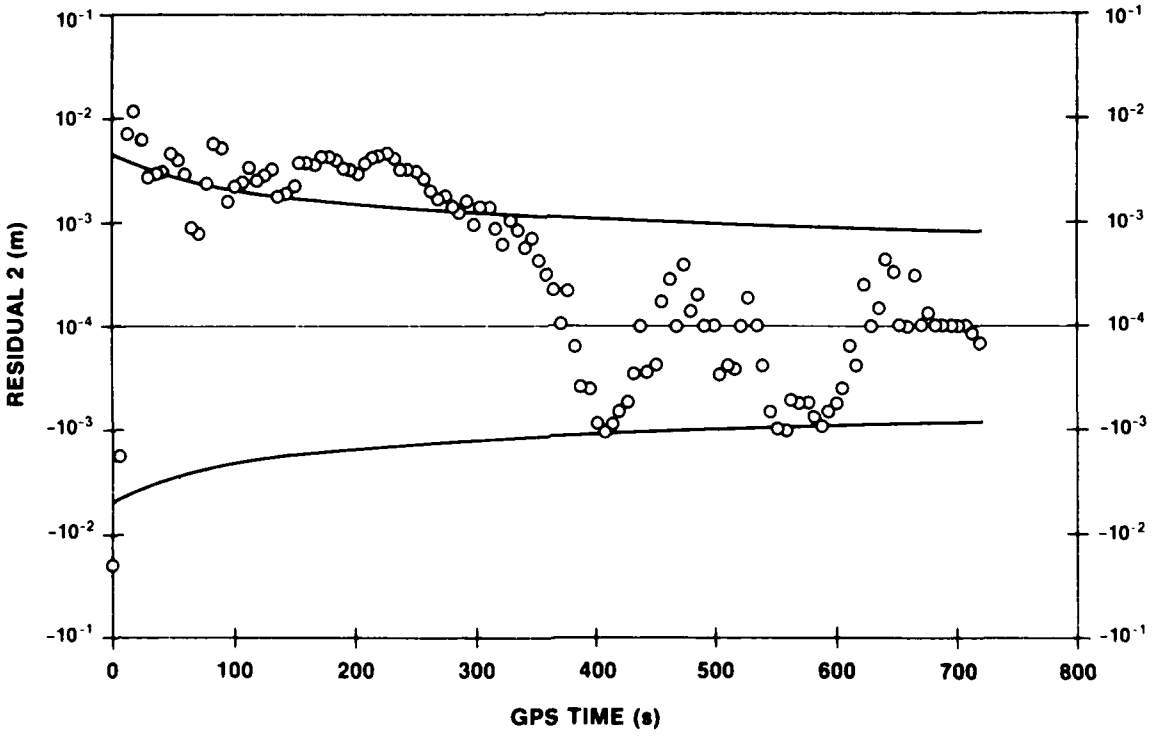

PLOT 8. ANTENNA 2 BIAS RESIDUAL, (ESTIMATE-TRUTH); 2-m ANTENNA BASELINES

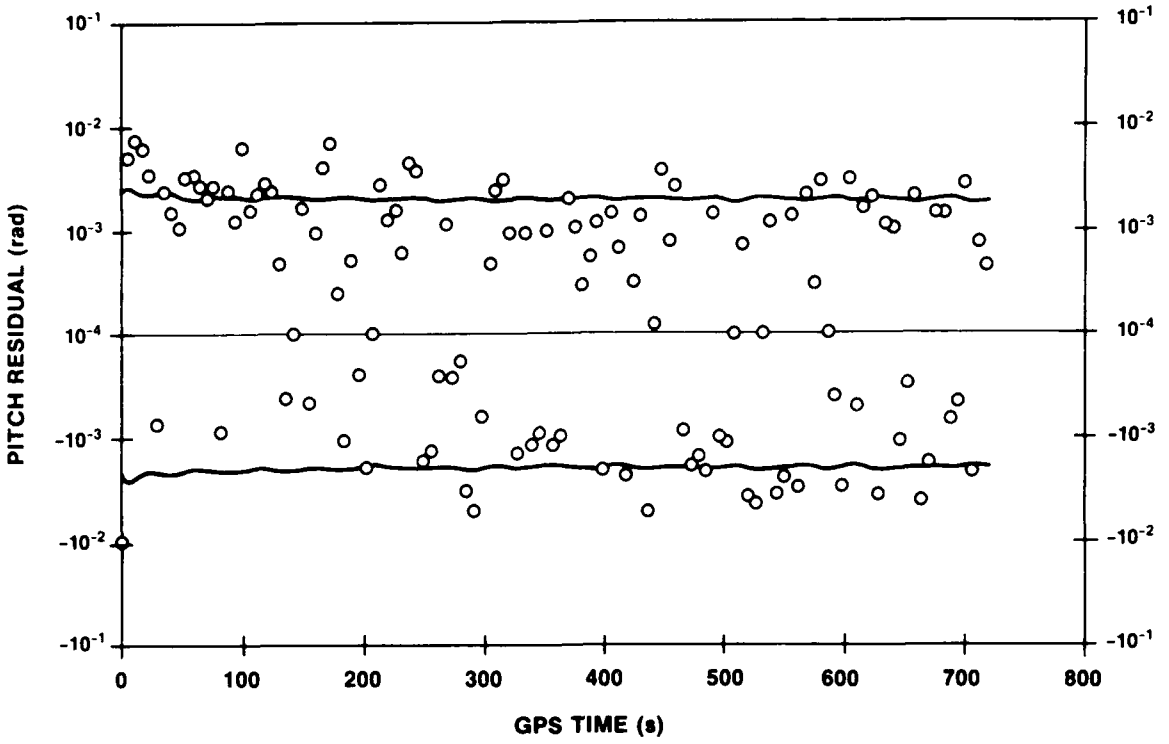

PLOT 5. ORIENTATION RESIDUALS, LOCAL VERTICAL PITCH (ESTIMATE-TRUTH); 2-m ANTENNA BASELINES

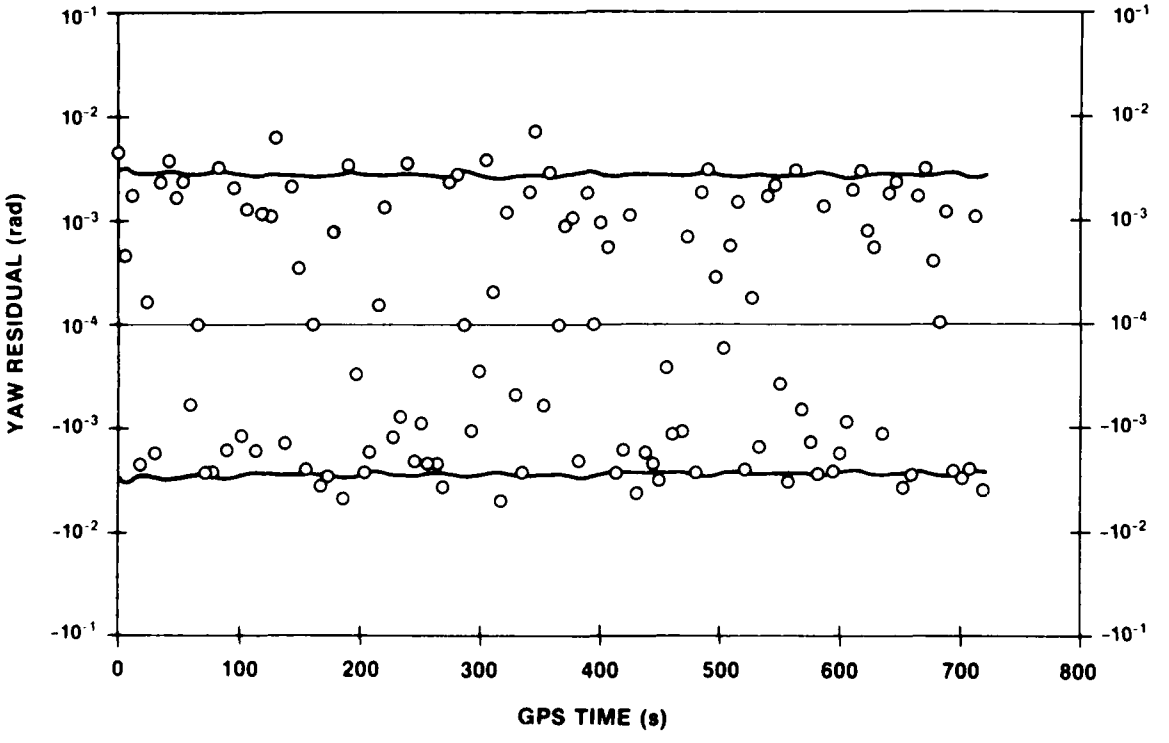

PLOT 6. ORIENTATION RESIDUALS, LOCAL VERTICAL YAW (ESTIMATE-TRUTH); 2-m ANTENNA BASELINES

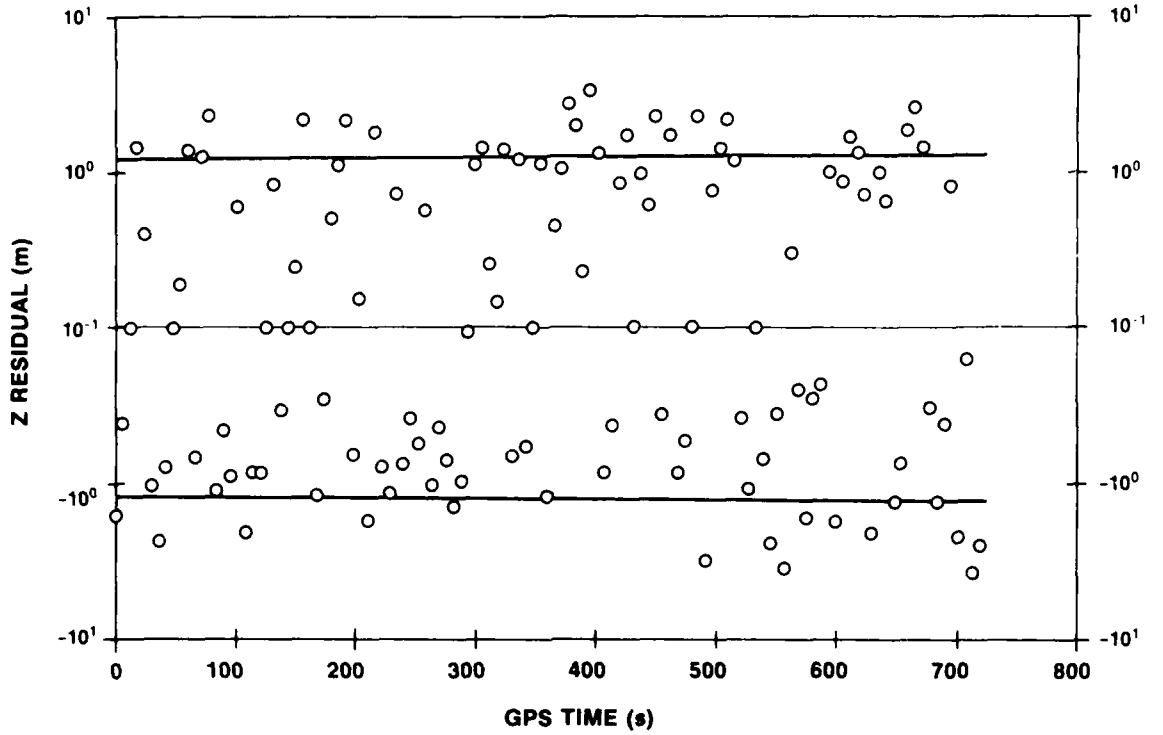

PLOT 3. NAVIGATION RESIDUALS, EARTH-FIXED Z (ESTIMATE-TRUTH); 2-m ANTENNA BASELINES

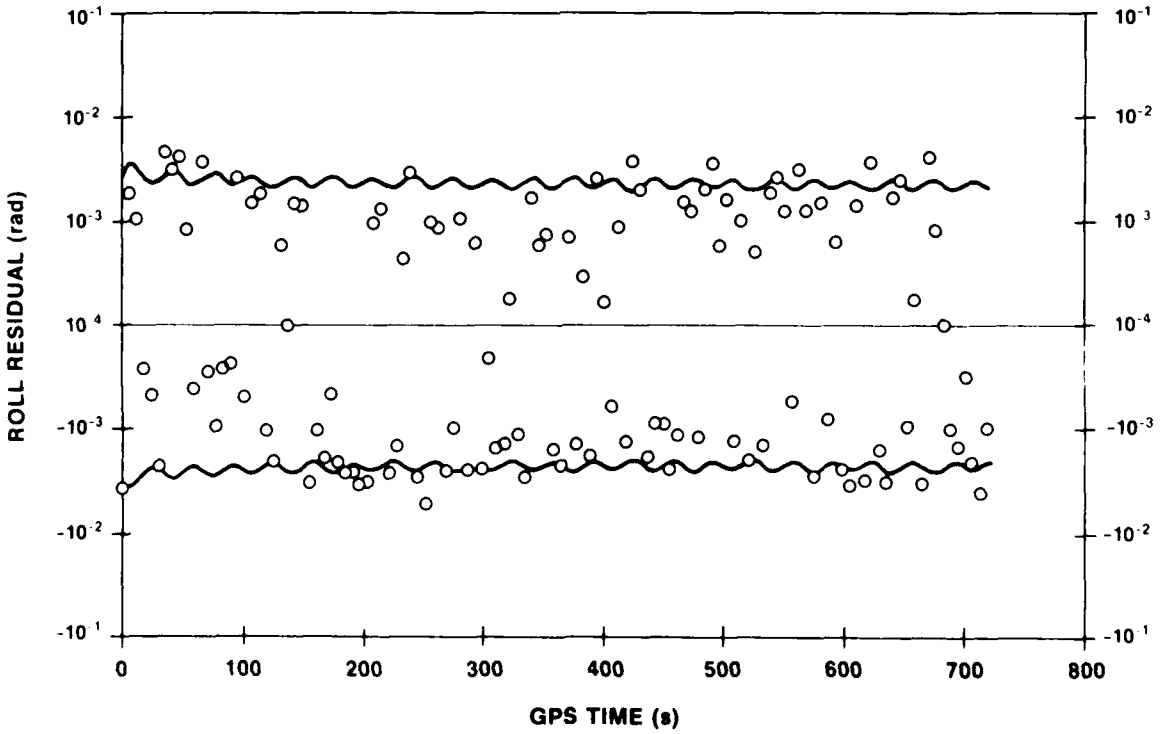

PLOT 4. NAVIGATION RESIDUALS, LOCAL VERTICAL ROLL (ESTIMATE-TRUTH); 2-m ANTENNA BASELINES

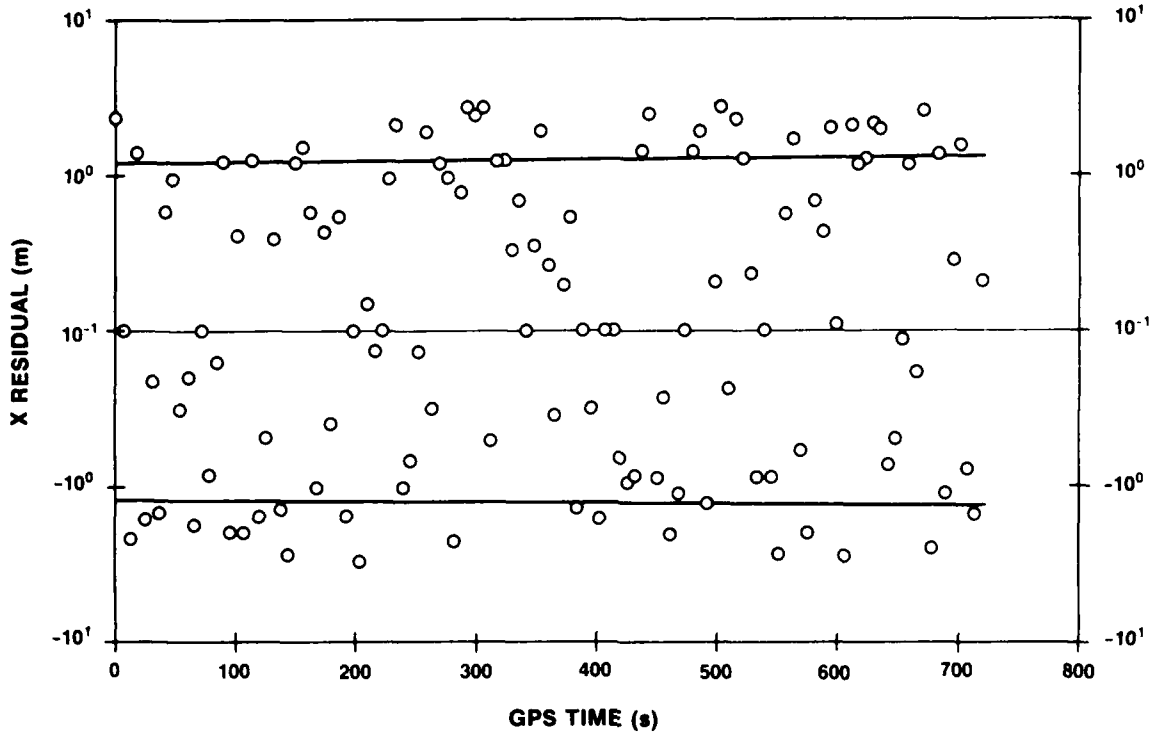

PLOT 1. NAVIGATION RESIDUALS, EARTH-FIXED X (ESTIMATE-TRUTH); 2-m ANTENNA BASELINES

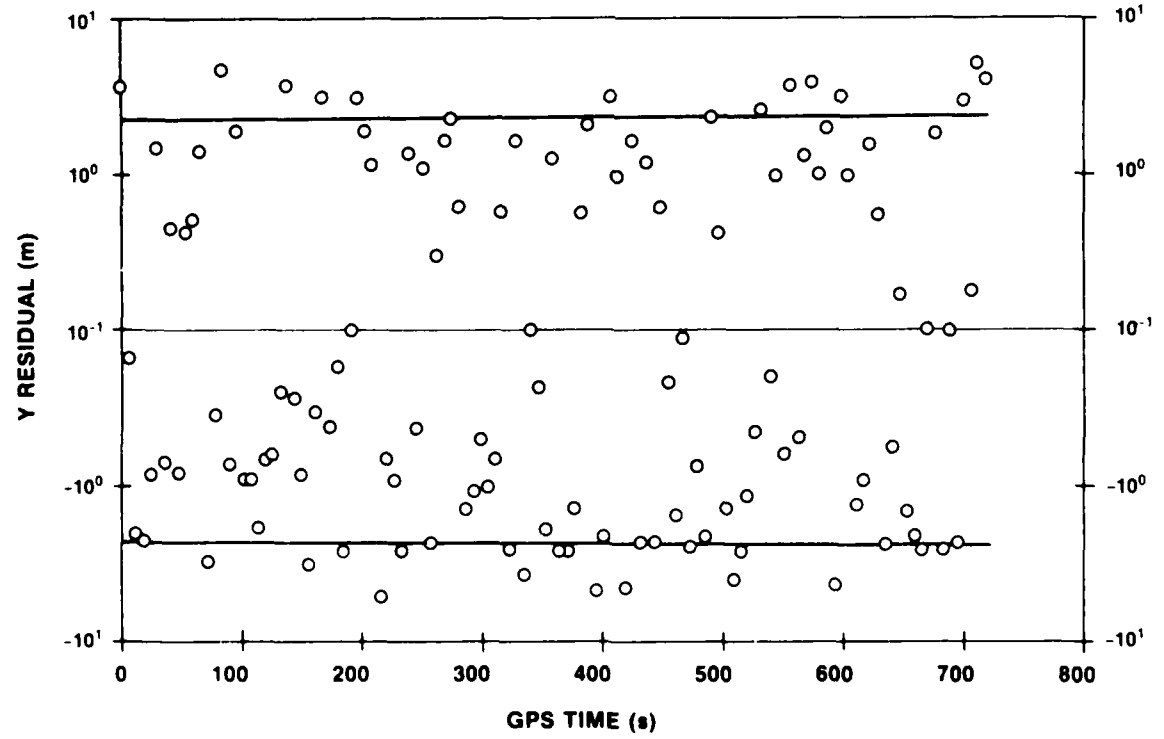

PLOT 2. NAVIGATION RESIDUALS, EARTH-FIXED Y (ESTIMATE-TRUTH); 2-m ANTENNA BASELINES

4. *Design Analysis Report III For The TI4100 GEOSTAR Receiver*, 23 December 1982.

5. P. Kruh, *The NAVSTAR Global Positioning System Six Plane 18-Satellite Constellation*, IEEE National Telecommunication Conference, New Orleans, 1981.

6. G.L. Mealy and D.R. Vander Steop, *Time Standard Error Modeling With Applications to Satellite Navigation*, Proc. 29th Annual Symposium on Frequency Control, May 1975, pp. 417-424.

model fits the cable behavior. Unpredictable phase variations due to kinks or thermal effects of sunlight and shadow are not modeled and must be examined separately.

Clearly, a larger baseline produces higher precision orientation capability for a given measurement accuracy. However, as noted above, longer baselines are prone to introduce unmodeled effects that may make the potential improvement unrealizable. This simulation demonstrates that the three-antenna array nominally separated by 20-m approaches 0.2 mrad resolution in the three angles for the given 0.5-cm phase measurement accuracy. As expected, the 2-m array is a factor of 10 worse. In general, the angular precision can be summarized by the following relationship:

$$\Delta \psi = \frac{\Delta l}{b} \csc \psi$$

where $\Delta \psi$ = angular precision (rad)
Δl = phase measurement error (m)
b = baseline length (m)
ψ = angle between the baseline vector and the vector to the satellite

Use of several satellites and two or more baselines will tend to minimize the effect of $\csc\psi$ in this equation. Thus, $\Delta l / b$ more nearly represents the standard deviation observed for roll, pitch, and yaw in this simulation.

CONCLUSION

All troublesome propagation effects have been neglected in this simulation and, consequently, the results represent a best case. Under these optimistic conditions, the simulation shows that milliradian angular solutions are feasible using the GPS and a suitable receiver such as the TI GEOSTAR. Submilliradian accuracies are also possible, but will require a distance between antennas of about 20-m. It is doubtful that additional improvements in phase measurement accuracy will buy a proportional amount of improvement in angular resolution. Effort should instead be placed toward improving the models of propagation effects, working to remove the mechanical instabilities of the antenna baseline on a moving vehicle, and controlling the thermal variations in long signal cables. Clever mechanical design and more sophisticated software will be needed to make 0.1-mrad orientations routine.

REFERENCES

1. R.J. Milliken and C.J. Zoller, "Principle of Operation of NAVSTAR and System Characteristics", NAVIGATION, Vol 25, #2, 1978.

2. P.W. Ward, *An Advanced NAVSTAR GPS Multiplex Receiver*, IEEE Position Location and Navigation Symposium, Atlantic City, N.J., 1980.

3. C.R. Johnson, P.W. Ward, M.D. Turner, and S.D. Roemerman, "Applications of a Multiplexed GPS User Set", NAVIGATION, Vol 28, #4, 1981.

simulation, longer baselines would continue to improve the angular resolution. However, practical considerations, discussed in the next section, would work in the opposite direction.

The antenna biases, initially unknown, gradually converge toward a small residual as data is accumulated. The bias residuals appear in Plots 8-9 and 18-19. As discussed previously, the knowledge of these states improves due to the accumulation of information over the span of observations. The effect of this improvement is reflected in the orientation residuals and can be seen particularly in the case of pitch (Plot 15). During the first 2 min of observations, the pitch residual is larger than it is later when the antenna bias residuals are reduced. It can also be seen in Plot 5, but the larger residuals make the effect less obvious. In both cases, the pitch component shows the effect more than roll or yaw because the correlation coefficients of pitch with respect to the antenna biases have the same sign. The correlation coefficients of roll and yaw with respect to the antenna biases have opposite sign and, consequently, tend to cancel each other when the antenna bias residuals are in the same sense.

DISCUSSION

This simulation demonstrates that the intrinsic measurement accuracy of the GPS signals readily meets the 20-m three-dimensional navigation error requirement of the application. However, there are many sources of measurement error, not included in the simulation, that are capable of biasing the result and its effects are difficult to detect.

Accurate prediction of the satellite trajectory over a long enough period of time with sufficient accuracy to make the broadcast ephemeris suitable for high-precision navigation and point positioning will continue to be a challenge. Improvement of our understanding of the forces acting on the satellites and an increase in the number of tracking stations may combine to decrease the size of the broadcast ephemeris error in the future. Closely related to the ephemeris error is the prediction of satellite time. Satellite clock corrections are included in the broadcast ephemeris and need to be considered as part of the ephemeris prediction problem.

Ionospheric refraction, tropospheric refraction, and relativity are biases that were not considered in this simulation. Errors here will particularly effect the navigation solution,since they, like ephemeris errors, can introduce time-varying radial signals that cannot be easily separated from the true signal. The orientation solution is not significantly degraded by these types of errors as long as the phase front remains intact across a dimension comparable to the longest antenna baseline length. However, warping of the phase front due to propagation effects so that arrival times at the antennas are perturbed would be of serious concern .

Any phenomena that differentially influences the arrival times of the signals from the several antennas at the receiver in an unexpected manner would produce errors in the orientation solution. Any movement of the antenna phase center as a function of the direction to a satellite must be measured and modeled. The distance between antenna phase centers (i.e., the respective baselines) and the orientation of the antenna array with respect to the vehicle must all be measured and remain stable to an accuracy better that that desired for the system performance. This requirement tends to favor short baselines and systems where all antennas are rigidly mounted on a single structure that can then be precisely mounted on the vehicle.

Propagation delays of signals from each antenna to the receiver can be accounted for in the antenna biases, if the effects are time-independent. Calibration of these signal cables will not be necessary as long as the

$$B_{ppk}\,\Delta\bar{x}_{pk} + B_{pbk}\,\Delta\bar{x}_{bk} = E_{pk}$$

$$B_{pbk}^{T}\,\Delta\bar{x}_{pk} + (B_{bbk} + D_{k-1})\,\Delta\bar{x}_{bk} = (E_{bk} + F_{k-1}) \qquad \text{(A-7)}$$

Solution at t_k proceeds by premultiplying both sides of the unpartitioned matrix equation by B^{-1}. The result is the vector $\Delta\bar{x}_k$ as desired.

CONSTRUCTION OF THE A MATRIX

As discussed above, two data classes are used to produce the combined position and orientation solution. The partial derivatives for each of these will be presented independently. Reference to the diagram in Appendix B (Figure B-1) will be helpful.

Pseudorange

The pseudorange observations can be modeled by the following equation:

$$\rho_{kij} = |\bar{r}_j - \bar{e}_i|_k + C\,[\tau_0 + \tau_i + \dot{\tau}_i\,(t_k - t_0)] \qquad i > 1 \qquad \text{(A-8)}$$

where subscript j = the satellite
subscript i = the antenna

The two vectors $\bar{e}_i$ and $\bar{r}_j$ (defined in Figure B-1) are the ECEF coordinates of the i th antenna and the ECEF coordinates of the j th satellite, respectively. The biases, represented by the taus in equation (A-8), are composites. The local clock bias τ_0 and the reference antenna biases τ_1 and $\dot{\tau}_1$ are grouped together to make a single Class 1 state ξ_0. The Class 2 states are the biases and drifts associated with the remaining antennas plus ξ_0. These effects arise due to cable variations, etc., and are represented by τ_i and τ_{i+} respectively ($i > 1$). The sum of all these effects is the total delay impressed upon the signal from each antenna. In summary, the biases are as follows:

reference antenna: $\xi_0 = \tau_0 + \tau_1 + \dot{\tau}_1\,(t_k - t_0)$

all other antennas: $\xi_0 + \tau_i + \dot{\tau}_i\,(t_k - t_0)$

Equation (A-8) is the observation equation for the pseudorange data class. It represents C_k, which was defined in the first section of this appendix. In order to form the A matrix, the partial derivative of ρ_{kij} is required with respect to each state variable:

$$e_{u1},\ e_{u2},\ e_{u3},\ \gamma_1,\ \gamma_2,\ \gamma_3,\ \xi_0,\ \tau_1,\ \ldots\ \tau_{na},\ \dot{\tau}_1,\ \ldots\ \dot{\tau}_{na}$$

The partial derivatives with respect to these states are written below, with the subscript m indicating the coordinate, m = 1, 2, 3.

$$\frac{\partial \rho_{kij}}{\partial e_{u,m}} = -\frac{(r_{x1} - e_{x1})\,\dfrac{\partial e_{x1}}{\partial e_{um}} + (r_{y1} - e_{y1})\,\dfrac{\partial e_{y1}}{\partial e_{um}} + (r_{z1} - e_{z1})\,\dfrac{\partial e_{z1}}{\partial e_{um}}}{|\bar{r}_j - \bar{e}_i|_k}$$

$$\frac{\partial \rho_{kji}}{\partial \gamma_m} = - \frac{(r_{xj} - e_{xi}) \frac{\partial e_{xi}}{\partial \gamma_m} + (r_{yj} - e_{yi}) \frac{\partial e_{yi}}{\partial \gamma_m} + (r_{zj} - e_{zi}) \frac{\partial e_{zi}}{\partial \gamma_m}}{| \bar{r}_j - \bar{e}_i |_k}$$

$$\frac{\partial \rho_{kji}}{\partial \xi_0} = \frac{\partial \rho_{kji}}{\partial \tau_i} = c \qquad i > 1$$

$$\frac{\partial \rho_{kji}}{\partial \dot{\tau}_i} = c(t_k - t_0) \qquad i > 1$$

The result from Appendix B, equation (B-1) is required to evaluate the partials of the antenna positions with respect to the states. The partial of equation (B-1) with respect to coordinates follows:

$$\frac{\partial \bar{e}_i}{\partial e_{um}} = \left[T_{eu} \frac{\partial T_{uv}}{\partial e_{um}} + \frac{\partial T_{eu}}{\partial e_{um}} T_{uv} \right] T_{vb} \bar{b}_i$$

Since T_{uv} is independent of $\bar{e}_i$ (Figure B-3), the above matrix equation reduces to

$$\frac{\partial \bar{e}_i}{\partial e_{um}} = \frac{\partial T_{eu}}{\partial e_{um}} T_{uv} T_{vb} \bar{b}_i \qquad m = 1, 2, 3$$

The evaluation of $\partial T_{eu} / \partial e_{um}$ is presented in Figure A-1; the form of T_{eu}, T_{uv}, and T_{vb} are given in Appendix B.

The partial of equation (B-1) with respect to the orientation angles roll, pitch, and yaw follows:

$$\frac{\partial \bar{e}_i}{\partial \gamma_m} = \left[T_{eu} \frac{\partial T_{uv}}{\partial \gamma_m} + \frac{\partial T_{eu}}{\partial \gamma_m} T_{uv} \right] T_{vb} \bar{b}_i$$

In this case, $\partial T_{eu} / \partial \gamma_m = 0$, and this allows the above matrix equation to be simplified to

$$\frac{\partial \bar{e}_i}{\partial \gamma_m} = T_{eu} \frac{\partial T_{uv}}{\partial \gamma_m} T_{vb} \bar{b}_i \qquad m = 1, 2, 3$$

The evaluation of $\partial T_{uv} / \partial \gamma_m$ is presented in Figure A-2. All these pieces can be put together to form the required partial derivatives.

Phase Difference

The observation equation for the phase difference data class can be obtained by subtracting the phase predicted at the reference antenna from the phase at all the other antennas:

$$\Delta \rho_{kji} = \rho_{kji} - \rho_{kj1} \qquad i > 1 \qquad \text{(A-9)}$$

The expansion of the above, using equation (A-B), is

$$\Delta\rho_{kii} = |\bar{r}_i - \bar{e}_i|_k - |\bar{r}_i - \bar{e}_i|_k + c[\tau_i + \dot{\tau}_i (t_k - t_0)] \qquad i > 1 \qquad \text{(A-10)}$$

The partial derivatives can be fashioned from the previous results and equations (A-9) and (A-10).

$$\frac{\partial\Delta\rho_{kii}}{\partial e_{um}} = \frac{\partial\rho_{kii}}{\partial e_{um}} - \frac{\partial\rho_{kil}}{\partial e_{um}} \qquad i > 1 \qquad m = 1, 2, 3$$

$$\frac{\partial\Delta\rho_{kii}}{\partial\gamma_{um}} = \frac{\partial\rho_{kii}}{\partial\gamma_{um}} - \frac{\partial\rho_{kjl}}{\partial\gamma_{um}} \qquad i > 1 \qquad m = 1, 2, 3$$

$$\frac{\partial\Delta\rho_{kii}}{\partial\xi_0} = 0$$

$$\frac{\partial\Delta\rho_{kii}}{\partial\tau_i} = c \qquad i > 1$$

$$\frac{\partial\Delta\rho_{kii}}{\partial\dot{\tau}_i} = c(t_k - t_0) \qquad i > 1$$

$$\frac{\partial T_{eu}}{\partial \bar{e}_u} = \begin{vmatrix} -\xi_1 & -\xi_4\cos\lambda - \xi_2\sin\beta & \xi_3\cos\lambda + \xi_2\cos\beta & k_1 \\ \xi_2 & -\xi_4\sin\lambda - \xi_1\sin\beta & \xi_3\sin\lambda + \xi_1\cos\beta & k_2 \\ 0 & \xi_3 & \xi_4 & k_3 \\ 0 & 0 & 0 & 0 \end{vmatrix}$$

$$\frac{\partial T_{eu}}{\partial e_{u1}} : \begin{cases} r_1 = -\dfrac{e_{u1}\,e_{u2}}{r^3} & \xi_1 = -\dfrac{e_{u1}\,e_{u3}}{R^3} & k_1 = 1 \\ \xi_2 = -\dfrac{e_{u1}^2}{r^3} + \dfrac{1}{r} & \xi = -\dfrac{e_{u1}r}{R^3} + \dfrac{e_{u1}}{Rr} & k_2 = k_3 = 0 \end{cases}$$

$$\frac{\partial T_{eu}}{\partial e_{u2}} : \begin{cases} \xi_1 = -\dfrac{e_{u2}^2}{r^3} + \dfrac{1}{r} & \xi_3 = -\dfrac{e_{u1}e_{u3}}{R^3} & k_2 = 1 \\ \xi_2 = -\dfrac{e_1\,e_{u2}}{r^3} & \xi_4 = -\dfrac{e_{u2}\,r}{R^3} + \dfrac{e_{u2}}{Rr} & k_1 = k_3 = 0 \end{cases}$$

$$\frac{\partial T_{eu}}{\partial e_{u3}} : \begin{cases} \xi_1 = 0 & \xi_3 = -\dfrac{e_{u3}^2}{R^3} + \dfrac{1}{R} & k_3 = 1 \\ \xi_2 = -0 & \xi_4 = -\dfrac{e_{u3}\,r}{R^3} & k_1 = k_2 = 0 \end{cases}$$

$$r = [e_{u1}^2 + e_{u2}^2]^{1/2} \qquad R = [r^2 + e_{u3}^2]^{1/2}$$

FIGURE A-1. PARTIALS OF T_{eu} WITH RESPECT TO COORDINATE STATES $\bar{e}_u$

$$\frac{\partial T_{ws}}{\partial T\gamma_1} = \begin{bmatrix} -\cos\gamma_3\sin\gamma_1 - \sin\gamma_1\sin\gamma_2\cos\gamma_3 & 0 & \cos\gamma_3\cos\gamma_1 - \sin\gamma_3\sin\gamma_2\sin\gamma_1 & 0 \\ -\sin\gamma_3\sin\gamma_1 + \cos\gamma_1\sin\gamma_2\cos\gamma_3 & 0 & \sin\gamma_3\cos\gamma_1 + \cos\gamma_3\sin\gamma_2\sin\gamma_1 & 0 \\ -\cos\gamma_2\cos\gamma_1 & 0 & -\cos\gamma_2\sin\gamma_1 & 0 \\ 0 & 0 & 0 & 0 \end{bmatrix}$$

$$\frac{\partial T_{ws}}{\partial T\gamma_2} = \begin{bmatrix} -\sin\gamma_3\cos\gamma_2\sin\gamma_1 & \sin\gamma_1\sin\gamma_2 & \sin\gamma_3\cos\gamma_2\cos\gamma_1 & 0 \\ \cos\gamma_3\cos\gamma_2\sin\gamma_1 & -\cos\gamma_3\sin\gamma_2 & -\cos\gamma_3\cos\gamma_2\cos\gamma_1 & 0 \\ \sin\gamma_2\sin\gamma_1 & \cos\gamma_2 & -\sin\gamma_2\cos\gamma_1 & 0 \\ 0 & 0 & 0 & 0 \end{bmatrix}$$

$$\frac{\partial T_{ws}}{\partial T\gamma_3} = \begin{bmatrix} -\sin\gamma_3\cos\gamma_1 - \cos\gamma_3\sin\gamma_2\sin\gamma_1 & -\cos\gamma_3\cos\gamma_2 & -\sin\gamma_3\sin\gamma_1 + \cos\gamma_3\sin\gamma_2\cos\gamma_1 & 0 \\ \cos\gamma_3\cos\gamma_1 - \sin\gamma_3\sin\gamma_2\sin\gamma_1 & -\cos\gamma_2\sin\gamma_3 & \cos\gamma_3\sin\gamma_1 + \sin\gamma_3\sin\gamma_2\cos\gamma_1 & 0 \\ 0 & 0 & 0 & 0 \\ 0 & 0 & 0 & 0 \end{bmatrix}$$

FIGURE A-2. PARTIALS OF T_{ws} WITH RESPECT TO ORIENTATION ANGLES

APPENDIX B

COORDINATE TRANSFORMATIONS

The GPS broadcast ephemeris provides the user with the satellite position in the earth-fixed coordinate system[1]. To be able to perform the least squares differential correction algorithm described in this report, one must be able to calculate the receiver antenna positions in the same system. The locations of the antennas are assumed to be surveyed in some convenient local reference frame. The relationship of this frame to the earth-fixed frame is the subject of this appendix.

The diagram in Figure B-1 shows two antennas: one at B_1 and one at B_i. One satellite is at P_j in the earth centered earth-fixed (ECEF) coordinate system. The vector $\bar{e}_i$ represents the coordinates of the i th antenna location, the vector $\bar{r}_j$ represents the j th satellite location, and the baseline vector $\bar{s}_i$ connects the reference antenna (I = 1) to the i th antenna. These relationships are described mathematically in the figure.

The observations consist of pseudoranges and phase differences. The pseudoranges include the geometric ranges h_{ij} plus the antenna biases τ_i and the local clock offset τ_0. The phase differences include the segment l_{ij} plus the difference in antenna offsets $\tau_i - \tau_1$. These observations, obtained from three or more antennas and four satellites, are required to produce a solution.

The antenna locations are defined in a reference frame independent of the vehicle. This reference frame is the b_1, b_2, b_3 frame drawn in Figure B-2. Each antenna has coordinates B_i (b_{1i}, b_{2i}, b_{3i}) in this baseline system. The vehicle reference frame is represented by the v_1, v_2, v_3, coordinates. The baseline system is rigidly attached to the vehicle system, but is translated by v_b and rotated by the angles θ_1 and θ_2. The vector $\bar{v}_b$ and the angles θ_1 and θ_2 are assumed to be known. The transformation matrix T_{vb}, which relates any point in the baseline system to its equivalent in the vehicle system, is presented in Figure B-2.

In a quiescent state, the vehicle system and the local vertical system would be coincident. However, under dynamic conditions, roll, pitch, and yaw are permitted; therefore, the vehicle system can rotate about each axis as illustrated in Figure B-3. These rotations are the orientation angles of the vehicle system with respect to the local vertical and are states of the solution vector. The transformation matrix T_{uv}, which transforms any point in the vehicle system to its equivalent in the local vertical system, is also presented in Figure B-3. Note that the first three rows of the fourth columns are zero. This indicates that there is no translation and so the origins always coincide.

A third transformation relates the local vertical to the ECEF coordinate system. Figure B-4 shows that the local vertical system is right handed with the u_3 axis positive in the radial direction and u_1 positive eastward. It

[1] A.J. Van Dierendonck, S.S. Russell, E.R. Kopitzke, and M. Birnbaum, "The GPS Navigation Message", NAVIGATION, Vol 25, #2, 1978.

is translated from the origin of the ECEF system by the vector $\bar{e}_u$ and rotated by λ and β. The $\bar{e}_u$ vector joins the origin of the two coordinate systems and is different from $\bar{e}_i$ in Figure B-1, which joins the origin of the ECEF system to each antenna. The angles λ and β are, respectively, the longitude and latitude of the vehicle origin and can be computed if $\bar{e}_u$ is known. The elements of the vector $\bar{e}_u$ are state elements, and along with roll, pitch, yaw, and the local clock bias, complete the first class of states described in Appendix A. The transformation matrix T_{eu}, which relates any point in the local vertical system to its equivalent in the ECEF system, is shown in Figure B-4.

These three transformations together transform the local antenna coordinates $\bar{b}_i$ into the ECEF coordinate system $\bar{e}_i$:

$$\bar{e}_i = T_{eu}\, T_{uv}\, T_{vb}\, \bar{b}_i \tag{B-1}$$

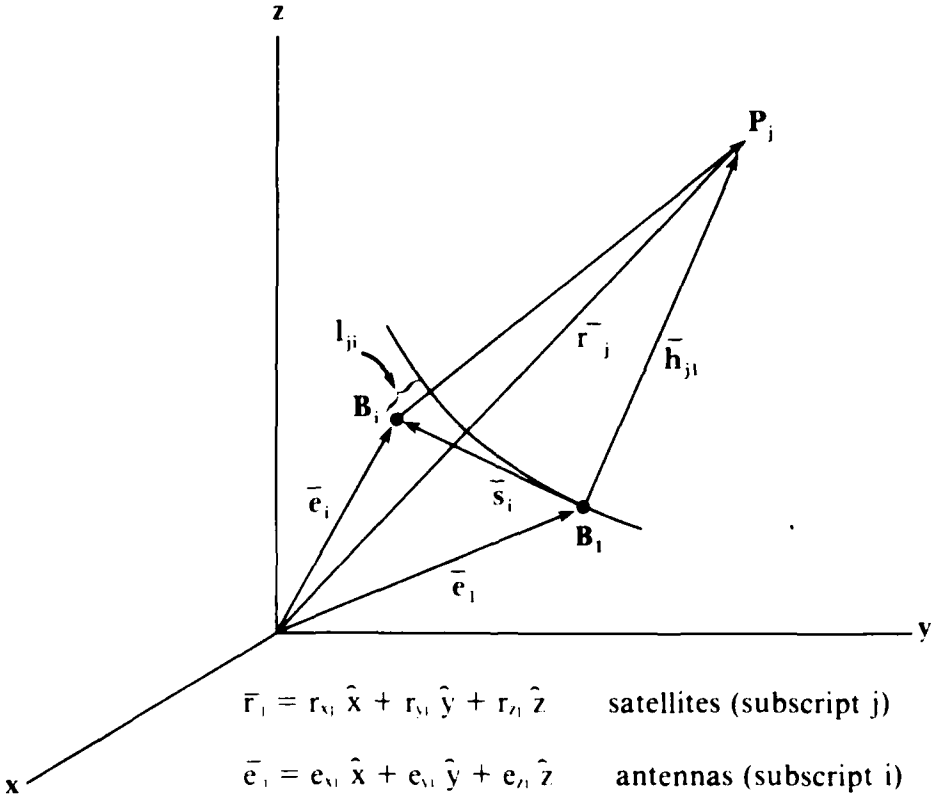

$\bar{r}_j = r_{xj}\,\hat{x} + r_{yj}\,\hat{y} + r_{zj}\,\hat{z}$ satellites (subscript j)

$\bar{e}_i = e_{xi}\,\hat{x} + e_{yi}\,\hat{y} + e_{zi}\,\hat{z}$ antennas (subscript i)

$\bar{h}_{ji} = (r_{xj} - e_{xi})\,\hat{x} + (r_{yj} - e_{yi})\,\hat{y} + (r_{zj} - e_{zi})\,\hat{z}$

$\bar{s}_i = (e_{xi} - e_{x1})\,\hat{x} + (e_{yi} - e_{y1})\,\hat{y} + (e_{zi} - e_{z1})\,\hat{z}\,, \qquad i \neq 1$

$h_{ji} = l_{ji} + h_{j1}$

FIGURE B-1. ANTENNAS AND SATELLITES IN THE ECEF COORDINATE SYSTEM

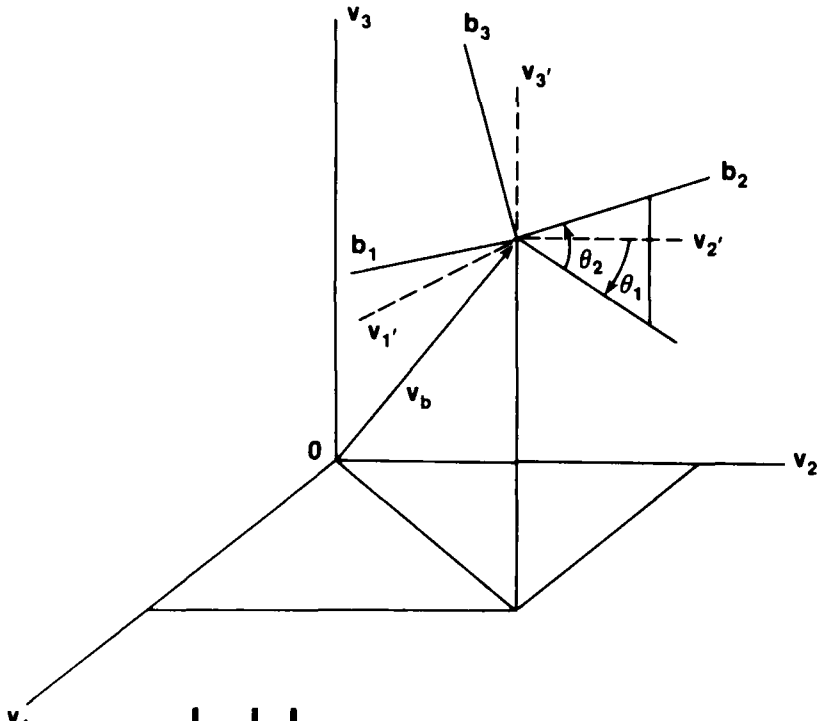

$$\begin{vmatrix} v_1 \\ v_2 \\ v_3 \\ v_S \end{vmatrix} = \begin{vmatrix} \cos\theta_1 & \sin\theta_1 \cos\theta_2 & -\sin\theta_1 \sin\theta_2 & v_{b1} \\ -\sin\theta_2 & \cos\theta_1 \cos\theta_2 & -\cos\theta_1 \sin\theta_2 & v_{b2} \\ 0 & \sin\theta_2 & \cos\theta_2 & v_{b3} \\ 0 & 0 & 0 & 1 \end{vmatrix} \bullet \begin{vmatrix} b_1 \\ b_2 \\ b_3 \\ 1 \end{vmatrix}$$

FIGURE B-2. TRANSFORMATION T_{vb}: BASELINE SYSTEM IN VEHICLE SYSTEM

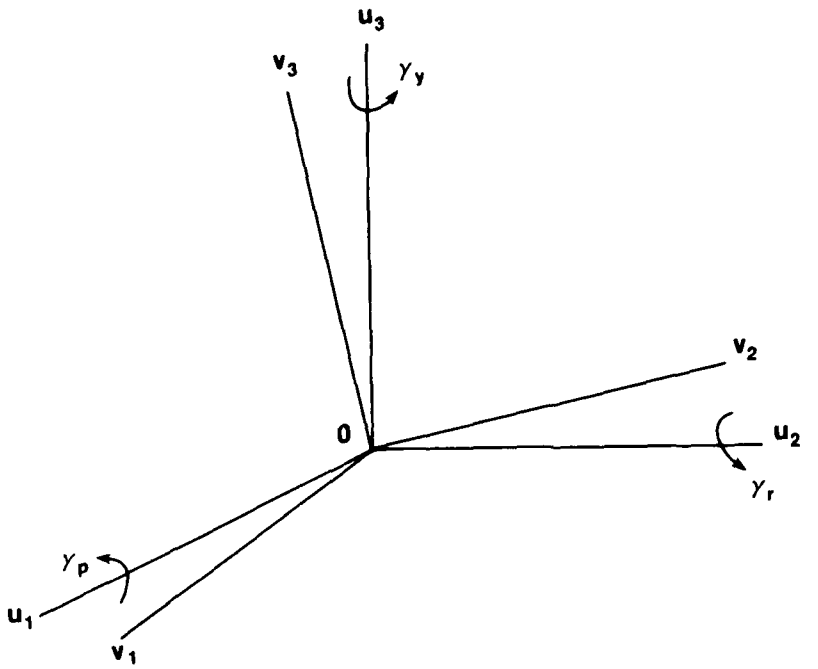

$$\begin{vmatrix} u_1 \\ u_2 \\ u_3 \\ u_x \end{vmatrix} = \begin{vmatrix} \cos\gamma_y \cos\gamma_r - \sin\gamma_y \sin\gamma_p \sin\gamma_r & -\sin\gamma_y \cos\gamma_p & \cos\gamma_y \sin\gamma_r + \sin\gamma_y \sin\gamma_p \cos\gamma_r & 0 \\ \sin\gamma_y \cos\gamma_r + \cos\gamma_y \sin\gamma_p \sin\gamma_r & \cos\gamma_y \cos\gamma_p & \sin\gamma_y \sin\gamma_r - \cos\gamma_y \sin\gamma_p \cos\gamma_r & 0 \\ -\cos\gamma_p \sin\gamma_r & \sin\gamma_p & \cos\gamma_p \cos\gamma_r & 0 \\ 0 & & 0 & 1 \end{vmatrix} \cdot \begin{vmatrix} v_1 \\ v_2 \\ v_3 \\ v_s \end{vmatrix}$$

FIGURE B-3. TRANSFORMATION T_{uv}: VEHICLE SYSTEM IN LOCAL VERTICAL

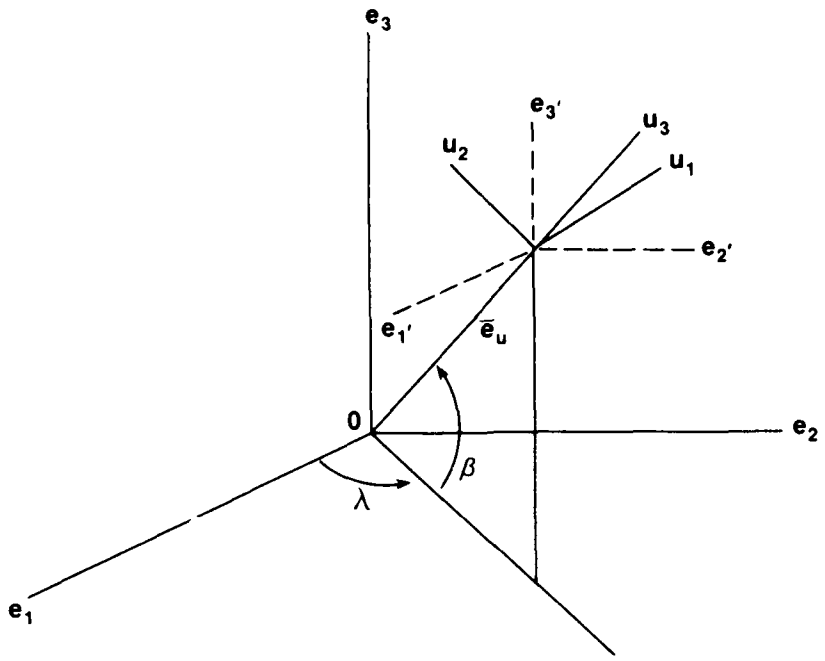

$$\begin{vmatrix} e_1 \\ e_2 \\ e_3 \\ e_s \end{vmatrix} = \begin{vmatrix} -\sin\lambda & -\cos\lambda\,\sin\beta & \cos\lambda\,\cos\beta & e_{u1} \\ \cos\lambda & -\sin\lambda\,\sin\beta & \sin\lambda\,\cos\beta & e_{u2} \\ 0 & \cos\beta & \sin\beta & e_{u3} \\ 0 & 0 & 0 & 1 \end{vmatrix} \cdot \begin{vmatrix} u_1 \\ u_2 \\ u_3 \\ u_s \end{vmatrix}$$

FIGURE B-4. TRANSFORMATION T_{eu}: LOCAL VERTICAL IN ECEF SYSTEM

DISTRIBUTION

	Copies
National Oceanographic Atmospheric Administration 6001 Executive Blvd. Attn: OA/C1X8 (Mr. Clyde Goad) Rockville, MD 20852	1
TASC 6 Jacob Way Attn: Gary Matchett Reading, MA 01867	1
AFGL-PHP Hanscom AFB Attn: Jack Klobuchar Bedford, MA 01731	1
STI 1195 Bordeaux Drive Attn: J. J. Spilker, Jr. Sunnyvale, CA 94086	5
IBM 18100 Frederick Pike Attn: Fritz Byrne Gaithersburg, MD 20760	3
Applied Physics Laboratory Johns Hopkins University Attn: Reginal Rhue Joseph Wall Edward Prozeller Johns Hopkins Road Laurel, MD 20810	1 1 1
Defense Mapping Agency Headquarters U.S. Naval Observatory Building 56 Attn: Dr. W. J. Senus (STT) Mr. H. Heuerman Washington, DC 20305	1 1
Defense Mapping Agency Aerospace Center 2nd & Arsenal St. Attn: George Stentz St. Louis, MO 63118	1
Professor Charles Counselman, III 54-620 Massachusetts Institute of Technology 77 Massachusetts Ave. Cambridge, MA 02139	1
Dr. Peter Bender Joint Institute for Laboratory Astrophysics University of Colorado Boulder, CO 80302	1
Magnavox Research Laboratory 2829 Moricopa St. Attn: Mr. Tom Starsel Torrance, CA 90503	1
National Oceanographic Atmospheric Administration 6001 Executive Blvd. Attn: OA/C1X8 (CAPT John Bossler) Rockville, MD 20852	
Defense Mapping Agency Hydrographic/Topographic Center Code GST 6500 Brookes Lane Attn: Ben Roth Patric Fell Fran Varnum Dr. W. H. Wooden II Washington, DC 20315	1 1 1 1

DISTRIBUTION (Continued)

	Copies
U.S. Geological Survey 526 National Center 12201 Sunrise Valley Drive Attn: COL Paul E. Needham Reston, VA 22092	1
Library of Congress Attn: Gift and Exchange Division Washington, DC 20540	1
University of Texas Applied Research Laboratory P.O. Box 8029 Attn: Dr. Arnold Tucker Dr. James Clynch Austin, TX 78712	1 1
Naval Research Laboratory Code 7966 Building 53 Attn: James Buisson Washington, DC 20315	1
Transportation System Center DST 542 Kendall Square Attn: John Kraemer Cambridge, MA 02142	1
Commander Naval Sea Systmes Command Attn: SEA-06 PMS-400 Washington, DC 20362	1 1
Director Joint Cruise Missile Project Office Washington, DC 20362	1
RCA M.T.P. Code M645 Building 989 Attn: William N. Beal Patrick AFB, FL 32925	1
ESMC Code RSN Building 989 Attn: Leon Crocker Patrick AFB, FL 32925	3
Geospace Systems Corporation Wellesley Office Park, Suite G-30 20 William Street Attn: C. L. Bradley Wellesley, MA 02181	1
Local:	
E31 (BIDEP)	1
E411 (Hall)	1
E431	10
F34	1
F41 (Saffos)	5
F42 (Dickerson)	1
K10	6
K13 (Hermann)	16
K13 (Evans)	1
N20	1
N30	1

END

FILMED

7-85

DTIC